Journal of Materials Chemistry C

ROYAL SOCIETY OF CHEMISTRY

REVIEW

View Article Online
View Journal | View Issue

Cite this: J. Mater. Chem. C, 2022, 10, 13462

A brief review on device operations and working mechanisms of organic transistor photomemories

Suhendro Purbo Prakoso, Mei-Nung Chen and Yu-Cheng Chiu *

A memory cell based on a three-terminal device or so-called transistor has greatly drawn attention for decades owing to its superior memory behavior and more versatile electrical property modulation compared to conventional two-terminal device. Recent progress shows that by introducing a photoactive charge storage interlayer in between dielectric and active semiconducting channels, the electrical properties of such a device can be feasibly controlled with photons, rendering novel ultrafast photo-recovery or photo-writing non-volatile transistor memories. Numerous photoactive materials, diverse structures and micro-to-nano scale dimensions of the charge trapping layer, including the plausible physical mechanisms, have been investigated and proposed to significantly level up the memory behaviors. As a result, the transistor photomemory has been emerging in many potential applications. In this review, different photoactive materials for the charge trapping layer will be presented briefly yet comprehensively. The device framework and its working principles will be systematically discussed and distinguished according to their unique memory behavior and applications. We also introduce a new insight into the tunneling effect in assisting photo-assisted memory transistors as a new branch and research venue. Lastly, the potential applications benefitted from transistor photomemory are exemplified to further understand the organic transistor photomemory devices comprehensively.

Received 29th March 2022,
Accepted 27th May 2022

DOI: 10.1039/d2tc01271e

rsc.li/materials-c

1. Introduction

Transistor, as it stands for "trans resistor" or "transfer of resistor" device, is a unique electronic component that could precisely control the resistance/conductance across a

Department of Chemical Engineering, National Taiwan University of Science and Technology, Taipei 106, Taiwan. E-mail: ycchiu@mail.ntust.edu.tw

Suhendro Purbo Prakoso

Suhendro Purbo Prakoso received his PhD degree from Taiwan International Graduate Program on Sustainable Chemical Science & Technology (TIGP-SCST) in 2021 under the guidance of Prof. Chien-Lung Wang (Department of Applied Chemistry, National Yang Ming Chiao Tung University) and Prof. Yu-Tai Tao (Institute of Chemistry, Academia Sinica). Currently, he works as a postdoctoral fellow in Prof. Yu-Cheng Chiu's group. His current research interests involve the low-voltage, tunnelling-effect of photo-assisted transistor memory devices and novel photosensitive charge storage materials.

Mei-Nung Chen

Mei-Nung Chen obtained her MS. from the Department of Chemical Engineering, National Taiwan University of Science and Technology (NTUST) in 2021, under the supervision of Prof. Yu-Cheng Chiu. Her research interests include the fabrication and developments of transistor-structured memories and organic field-effect transistors.

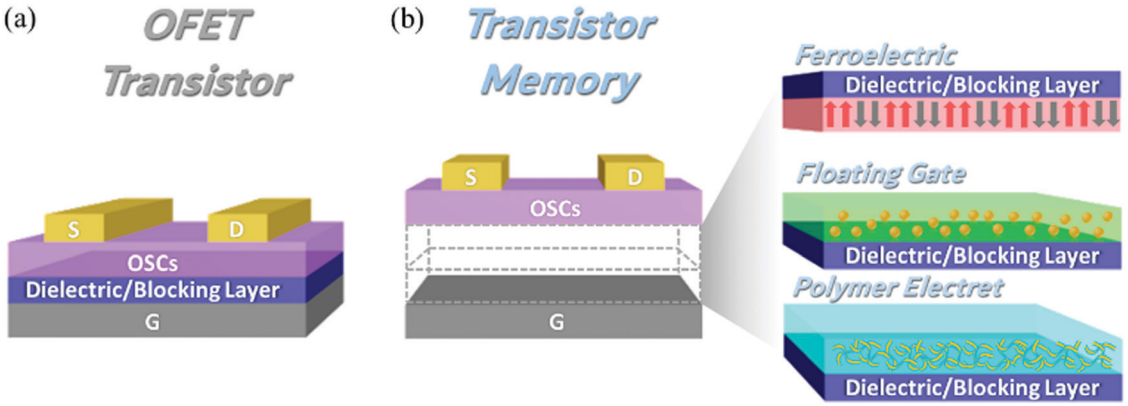

Fig. 1 (a) The conventional bottom-gate top-contact structure of an organic field-effect transistor (OFET) device. (b) The common structure of OFET memory devices with various polarization/charge storage layers.

semiconducting channel by finely tuning the strength of the electric field. Consequently, the device could regulate the current or voltage flow that acts as a switch or gain the electrical signals that are extremely useful to logic or analog circuitries, and many functional components.[1–3] The device possesses three terminals that are the so-called source (S), drain (D), and gate (G). In addition, in between the source/drain and gate, its conventional architecture has to contain a semiconductor and dielectric/blocking layer, as described in Fig. 1a.

As information technology has rapidly progressed, nowadays, many innovations in electronic components have also been developed specifically in response to the fields of the Internet of Things (IoT) and artificial intelligence (AI).[4–6] For instance, a high-density data storage,[7,8] a pulse monitoring sensor,[9] an artificial synapse,[10,11] a smart artificial retina,[12] a photorecorder,[13,14] pattern/image identification,[15,16] and an ultrasensitive photodetector;[17] all have been built-up based on a memory transistor framework. The clear difference between a memory transistor and a conventional one is in at least one additional polarization/charge storage layer that is sandwiched within the semiconductor and the gate contact (see Fig. 1b). This polarization/charge storage layer can extend the modulation of electrical behavior, thus establishing more pronounced hysteresis and/or threshold voltage shift (V_{th}) in the transfer characteristic of the transistor in order to incredibly improve memory performances.[18–20] In general, the transistor memories could be classified into three different types based on their polarization/charge storage materials,[21] as follows: (1) ferroelectric,[18,19] (2) floating-gate,[20,22–24] and (3) polymer electret transistor memory.[7,11,13,14] Among them, the polymer electret one can behave as a semi-permanent electric field and/or dipole moment that is formed by trapping electrostatic charges.[25,26] Besides this extraordinary function, the fabrication of transistor memory using polymer electrets is the most facile choice under solution processes and can be readily applied and adapted to many other processing methods from research scale to industrial applications.[27–30] As a result, rapid progress in the polymer electret-based transistor memories has been revealed.

Nevertheless, all of those memory devices typically operate under continuous/pulses electrical gate bias to control the memory behavior.[26] As such, it will cost more energy consumption, and more importantly, the transfer rate of the electrical signals will be limited to the speed of the charge transfer inside the circuitries.[31] A breakthrough has been made by incorporating photoactive materials into a polymer matrix[24] or *in situ* inheriting the photoactive properties of polymeric electrets *via* rational molecular design.[13,14,32] Since the photo-modulated transistor memory could allow high-speed optical signal transfer and less noise, bundling with low energy operation, this has becomes a new major direction in the field.[20] Such photoactive materials with optical physics properties (*e.g.*, optical band gap, emission lifetime, exciton generation/annihilation)[33] that benefit the transistor memories when the material interacts with light-matter (photon), establishing the novel transistor photomemory. The absorbed photons' energy in photoactive

Yu-Cheng Chiu

Yu-Cheng Chiu joined the Department of Chemical Engineering at Taiwan Tech. as a tenure-track assistant professor in August 2017. Prior to joining the faculty, Yu-Cheng was a postdoc in the Zhenan Bao research group at Stanford University, where he studied on developing intrinsically stretchable/healable semiconductor and high-performance OFET by solution shearing. Before moving to Stanford, he received his PhD degree under the supervision from Prof. Wen-Chang Chen in December 2012 from the Chem. E. at National Taiwan University and then stayed in the same group for his first post-doctoral research until 2014. Now Yu-Cheng's research focuses on elastic and self-healing semiconducting polymer, polymer transistor, transistor-based memory, and functional polymer materials.

materials will generate excitons (electron–hole pairs) that are directly involved in the charge trapping (charging electret) or recombination (neutralizing electret) process. Thus far, the device operations and its working principles have been discovered, such as photo-writing,[14] photo-recovery,[34] and else. Ultimately, the photonic transistor memory can be further operated partially[34] or even fully[10,35,36] by light to control the electrical properties of the device, which is in contrast to the electrically controlled alone.

Along with the countless variety of photoactive charge storage materials for transistor photomemories, the diverse structures, device operations, and physical mechanisms have been investigated and proposed, scrambling and piling up the abundance of new information in the field and producing the obscurity of its boundaries. Therefore, a clear classification of photonic transistor memories in terms of device operations and physical mechanisms that govern the memory behavior is required to serve as useful guidance. To the best of our knowledge, there have not been any reported cases in the field. In this review, we concisely elaborate the progress of photoactive materials used in organic transistor photomemories, as well as their device performances, and then systematically classify the physical device mechanisms in relation to their memory behavior and device operations. The present review will give hints for the design of organic transistor photomemories, and also offers to catalog each type that could assist the researchers in unfamiliar fields to clearly spot the differences of the device mechanisms, regardless of the photoactive charge storage layers employed in the device.

2. Basic operation of transistor memories and its important parameters

For the conventional transistor device (see Fig. 1a), assuming a p-type organic semiconducting (OSC) channel is employed, the application of an adequately high negative gate voltage (V_g) will induce the holes to accumulate at the bottom semiconductor interface and form the conductive accumulation region. At this stage, a negative voltage difference (V_{ds}) between the drain and source electrodes can drive the hole current in the accumulation mode, resulting in the high output drain current (I_d). This conventional transistor device is typically evaluated by measuring the transfer characteristic curve (I_d *vs.* V_g) and output characteristic curve (I_d *vs.* V_{ds}) as demonstrated in Fig. 2a and b, respectively. Accordingly, one of the important parameters to evaluate the transistor performances, that is, field-effect charge carrier mobility (μ) can be deduced from the slope of $I_d^{1/2}$ *vs.* V_g curve described in Fig. 2c.[37,38] The interception of its linear curve to the V_g axis will give the threshold voltage (V_{th}) value of the device, which is defined as the minimum V_g bias to stimulate the output I_d.

On the other hand, for the transistor memory, several additional parameters such as V_{th} shift (ΔV_{th}; memory window), memory ratio, retention time, endurance cycles and/or write-read-erase-read (WRER) cycles are essential to determine the performances of memory behavior.[26] A large V_{th} shift is highly desirable, which leads to a broad memory window and memory ratio to properly distinguish the memory levels. The V_{th} shift on transistor memory can be realized by the application of V_g bias at a time period that is so-called electrical "programming" or "erasing" (see Fig. 2d) depends on how the device behaves to the negative or positive V_g bias. This programming or erasing process will result in changes in the V_{th} and output I_d values when the device runs in the reading mode using the same fixed V_g and V_{ds}. The memory ratio is then determined by the ratio between high ("on" state) and low ("off" state) output I_d values. Not to mention that the output I_d values, either in the on or off state, have to be stable *i.e.*, the on or off state is utterly unchanged over time after programming or erasing treatment, reflecting the non-volatile memory type of the device. This capability can be evaluated through a retention time of at least 10^4 s (see Fig. 2e), and finally, as demonstrated in Fig. 2f, the WRER operations on the memory device can be also used to evaluate the stability and endurance of the dynamic changes in memory states.

Furthermore, in the photonic-based transistor memories, light exposure to the device at a time period (no bias on V_g and V_{ds}, merely illuminated by light) can also alter the V_{th} value.[33] Namely the process called, "photo-writing" or "photo-recovery" causes the V_{th} to shift away or come close to the initial state. Fig. 2g represents how the photo-writing or photo-recovery process shifts the V_{th} value of the device. Following the changes of V_{th} by light illumination, a simple evaluation to prove the authentication of photonic memory device is by monitoring the evolution of output I_d during a light pulse to the device as portrayed in Fig. 2h. Interestingly, aside from exposure time, the light properties that illuminate the photonic memory device also strongly affect the memory behavior, for instance, different light wavelengths (photon energy) and light intensities/powers.[39] Hence, this phenomenon ignites another important parameter named "photosensitivity"[8] and "photoresponsivity".[36] Although, both photosensitivity and photoresponsivity are defined as the changing portion of output I_d due to light irradiation, yet, the photoresponsivity may offer a better comparison study since the changes in output I_d are normalized by the incident illumination power.

3. Effects of photoactive charge storage materials on the memory characteristics

To date, plentiful photoactive materials have been explored and incorporated into the fabrication of high-performance photonic transistor memory devices. In brief, in this section, we will discuss some photonic memories employing various photoresponsive charge storage materials such as inorganic perovskite/insulated polymer blending based floating gates,[7,24,40–42] strong intramolecular donor–acceptor (D–A) and aggregation-induced-emission (AIE) conjugated polymer electrets,[13,14,32]

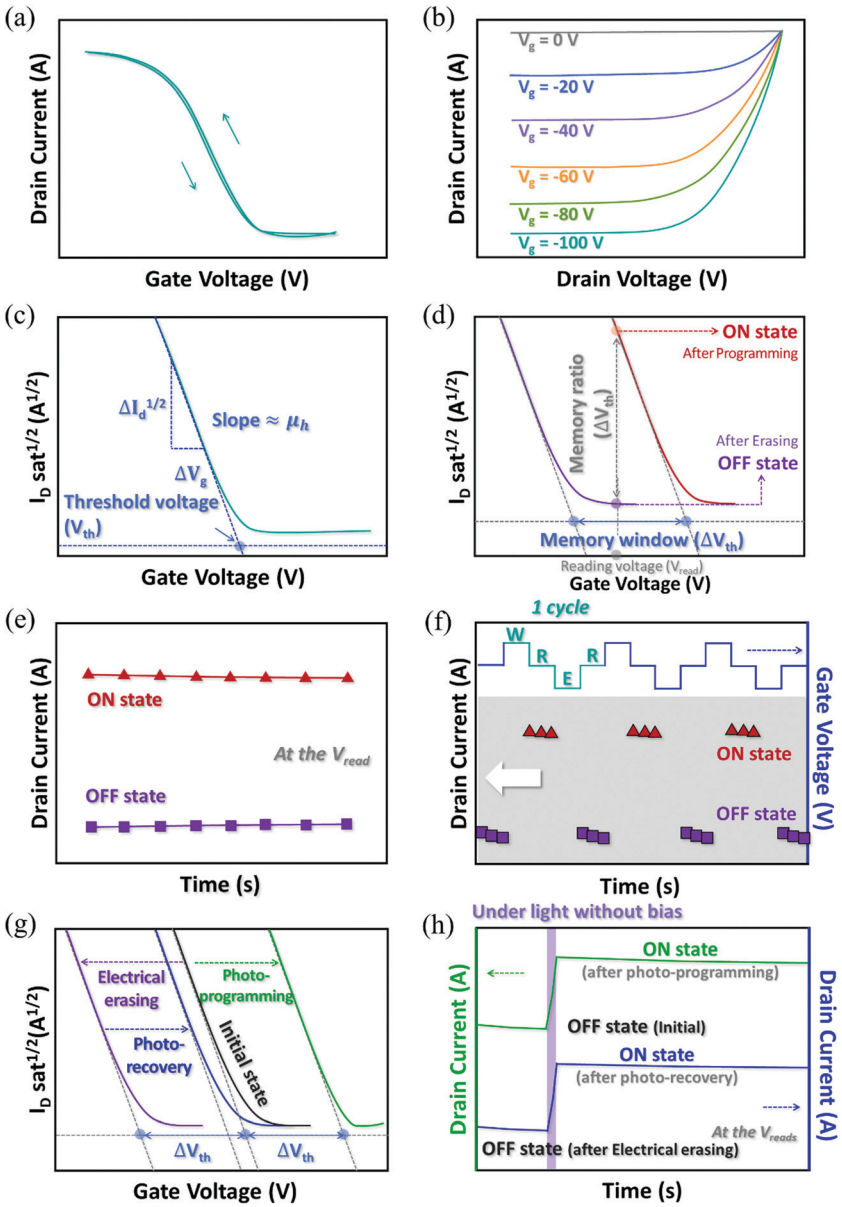

Fig. 2 The schematic plots for (a) transfer curve (I_d *vs.* V_g); (b) output curve (I_d *vs.* V_{ds}); (c) $I_d^{1/2}$ *vs.* V_g curve, to determine the charge carrier mobility (μ) and the threshold voltage (V_{th}); (d) $I_d^{1/2}$ *vs.* V_g curve for transistor memory operated after programming/erasing process to determine the ΔV_{th} of the memory window and memory ratio; (e) the retention curve showing the output I_d of on and off states over time; and (f) WRER cycle curve showing the memory device endurance over several cycles; (g) typical V_{th} changes on $I_d^{1/2}$ *vs.* V_g curve in photonic transistor memory operated after photo-writing/photo-recovery process; (h) output I_d evolution of the photomemory device after a light pulse.

and supramolecular based polymer electrets.[43–45] In the case of other photoactive charge storage material developments (such as rod-coil or rod-like liquid crystals, hybrid metal/metal-oxide nanoparticles/thin-films, metal–organic frameworks, photochromic blends/monolayers, biomass-derived electrets, and small-molecules based), and other unique morphologies/topologies of charge trapping interfaces, as well as device structures that are not covered in this section, could be found in the recently published reports and reviews.[22,23,46–58] Below, the device structures and its memory characteristics to the device operations will be elaborated in detail.

3.1. Blended perovskite/insulated polymer photoresponsive floating gates

Owing to the strong light-harvesting capability, low exciton binding energy, and long charge carrier lifetime (>100 ns) and diffusion length (>1 μm), inorganic perovskite-based materials have been chosen as versatile and promising photoresponsive materials.[24,40,59–63] For photomemory applications, typically perovskite nanoparticles (NPs) will be mixed with polymer insulation to control the film morphology and suppress the formation of the continuous perovskite film that might favor a pass way for depleting the trapped charges.[24,64]

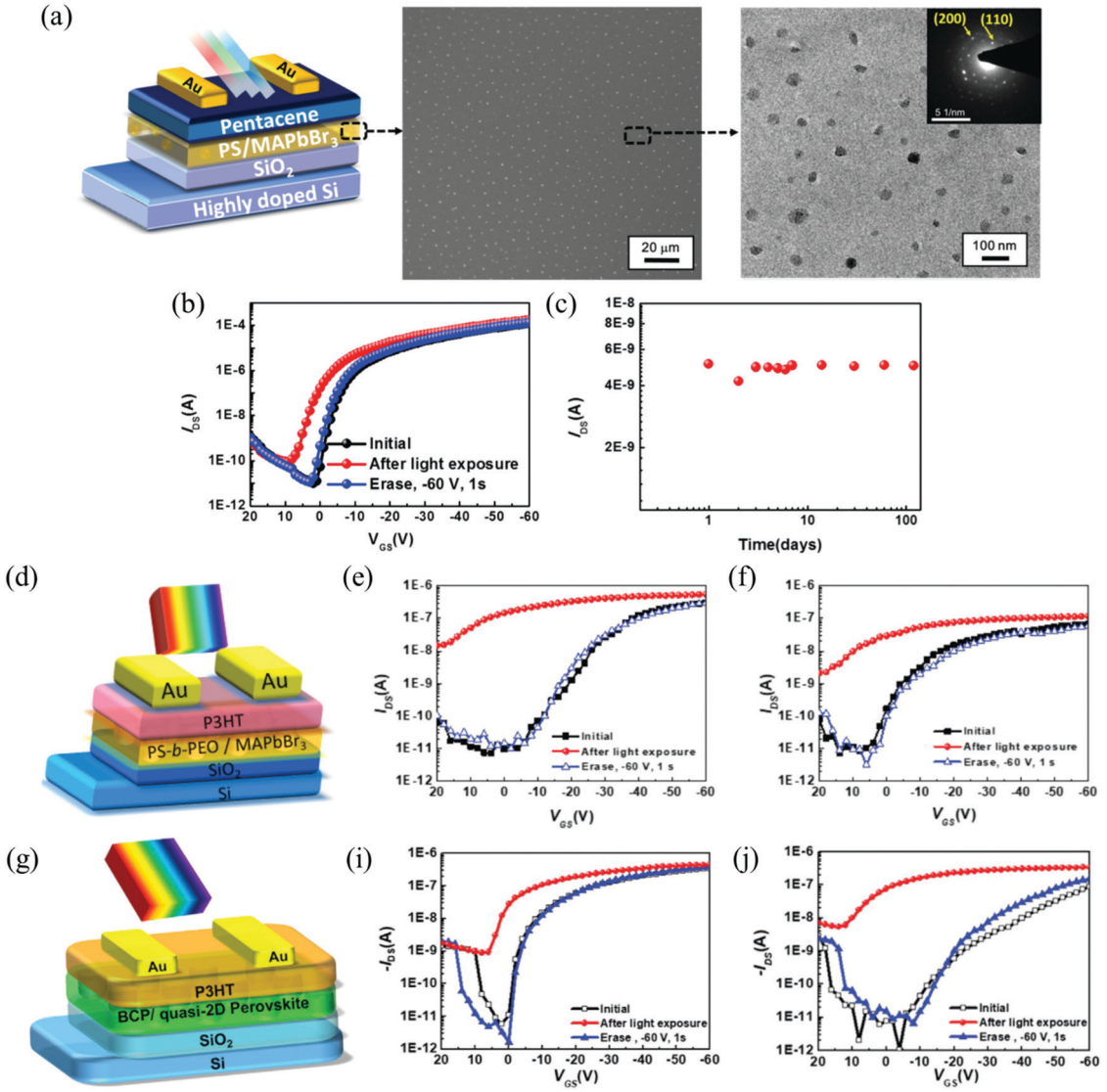

Fig. 3 (a, d and g) Show the device structures of various photonic memory devices using perovskite based floating gates. (b and c), e, f, i and j) show their associated transfer curves after different photo-writing treatments and electrical erasing processes. (a–c) Reprinted with permission from ref. 24. Copyright 2017 WILEY-VCH Verlag GmbH & Co. KGaA, Weinheim.[24] (d–f) Reprinted with permission from ref. 59. Copyright 2020 WILEY-VCH Verlag GmbH & Co. KGaA, Weinheim.[59] (g–j) Reprinted with permission from ref. 61. Copyright 2022 Wiley-VCH GmbH.[61]

By this method, the formation of the charge storage layer could be regarded as the floating gate type. The first work on this idea was actually reported by Chen *et al.* in 2017.[24] They blended $MAPbBr_3$ perovskite NPs with a polystyrene (PS) polymer matrix as the photoresponsive floating gate. Fig. 3a represents the device structure and the scanning electron microscopy (SEM) and transmission electron microscopy (TEM) images of the $MAPbBr_3$/PS composite film in the report. The SEM and TEM images clearly indicate the discrete formation and well-dispersed $MAPbBr_3$ NPs in the PS matrix, which can effectively strengthen the charge trapping capability to realize the non-volatile characteristics of the derived photomemory. As depicted in Fig. 3b, the manufactured device can exhibit a positive shift of V_{th} after the photo-writing process (UV light, 365 nm) for 120 s, implying that the perovskite blended PS floating gate can serve as the electron trapping sites. Fig. 3c demonstrates the memory retention time over three months after photo-writing, which further confirms the excellent charge storage stability. The neutralization of the photomemory device can be performed with electrical erasing by V_g of −60 V for 1 s, causing the transfer curve to shift back to the initial state. Following this study, Ercan *et al.* investigated the influence of different polymer matrices on the photoresponse and memory properties of perovskite-based photomemories.[64] In the report, all perovskite-based devices showed the transfer curve shift to the positive region after photo-writing treatment with blue light (450 nm) for 120 s. However, only two devices with polystyrene (PS) and poly(4-vinylphenol) (PVPh) host polymer matrixes can revert the transfer curve to the initial state *via* an electrical erasing process (at V_g of −60 V). Additionally, Chang *et al.* have

successfully fabricated a perovskite-based device with an exceptionally faster photo-writing time (*ca.* 5 ms) by introducing polystyrene-*block*-poly(ethylene oxide) (PS-*b*-PEO) as a polymer matrix shown in Fig. 3d.[59] The transfer curves of the devices also showed displacement towards the positive region upon the photo-writing process by green light (520 nm), displayed in Fig. 3e and f. With an erasing voltage pulse of about −60 V for 1 s, the device can be returned to its initial state, as caused by the charge neutralization due to hole injection. In a recent report, by adding phenylethylammonium bromide (PEABr) in polystyrene-*block*-poly(ethylene oxide) (PS-*b*-PEO)/$FAPbBr_3$ blends as the photoresponsive charge storage layer (see Fig. 3g), the degree of preferential orientation of perovskite crystallites towards the vertical axis can greatly enhance the charge transfer efficiency as well as the memory characteristics. It turned out that the same trend of transfer curve changes upon photo-writing (by blue light (450 nm), 240 s) and electrically erasing (at V_g of −60 V, 1 s) operations can be observed as illustrated in Fig. 3i and j.[61]

Unlike most transistor photomemories that partially rely on an electrical bias to perform a complete cycle of WRER, Liao *et al.* have conceptually developed a novel fully optically driven photomemory based on $Cs_2Pb(SCN)_2Br_2$ perovskite and poly(vinylpyrrolidone) (PVP) polymer blends seen in Fig. 4a.[35] The photo-writing and photo-recovery operations of the device can be attained by using two different light sources, *i.e.*, white

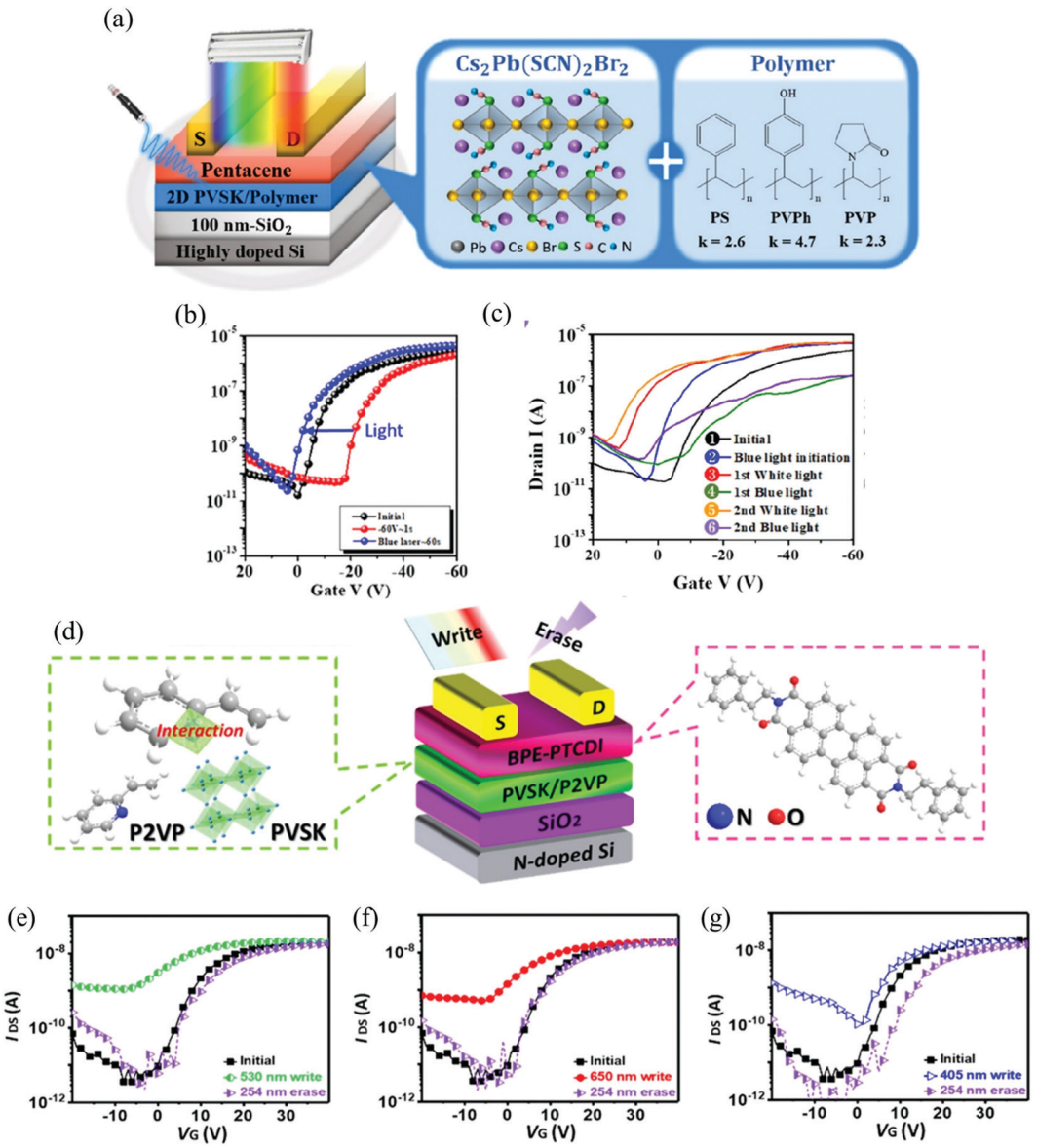

Fig. 4 (a and d) show the device structures of fully optical driven photomemory based floating gates along with the chemical motifs and perovskite structures. (b, c, e, f and g) show the respective transfer curves after treatment with various light wavelengths for photo-writing and photo-recovery processes. (a–c) Reprinted with permission from ref. 35. Copyright 2020 American Chemical Society.[35] (d–g) Reprinted with permission from ref. 36. Copyright 2021 American Chemical Society.[36]

Table 1 A comparison of the device performance of photoresponsive perovskite floating gates based photonic transistor memories with the SiO_2 blocking layer

SiO_2 thickness	Photoactive charge storage material	Programming/erasing operation (V)	Programming/erasing time (s)	ΔV_{th} (V)	I_{ON}/I_{OFF} ratio	Retention time (s)	Ref.
100	$MAPbBr_3$/PS	Light (365 nm)/−60	120/1	6.7	$\sim 10^4$	10^4	24
100	PVPh-pero	Light (450 nm)/−60	120/1	~31.5	$\sim 10^5$	$>10^3$	64
100	BCP-1/$MAPbBr_3$	Light (520 nm)/−60	240/1	—	$\sim 10^4$	10^4	59
100	PCDTPT/$CsPbBr_3$	Light (300 nm)/−10	0.5/0.1	66.5	$\sim 10^4$	10^4	41
100	$Cs_2AgBiBr_6$@OS	Light (450 nm)/−40	60/0.1	58	$\sim 10^4$	10^4	42
100	RP-17/βNC	Light (405 nm)/−60	120/1	18.34	$\sim 10^3$	$>10^4$	40
300	P3HT/FA-QDs	Light (520 nm)/−100	120/1	—	$\sim 10^4$	—	60
100	BCP/FAPbBr3–5% PEABr	Light (450 nm)/−60	240/1	—	$\sim 10^4$	10^4	61
100	$MAPbBr_3$/P2VP	Light (530 nm)/light (254 nm)	20/1	—	$\sim 10^4$	10^4	36

* Abbreviations: PS, Polystyrene; PVPh, poly(4-vinylphenol); pero, $CH_3NH_3PbBr_3$; BCP, block-copolymer; PCDTPT, poly[1,2,5]thiadiazolo[3,4-*c*]pyridine-4,7-diyl(4,4-dihexadecyl-4Hclopenta[2,1-*b*:3,4-*b*0]dithiophene-2,6-diyl)[1,2,5]thiadiazolo[3,4-*c*]pyridine-7,4-diyl(4,4-dihexadecyl-4*H*-cyclopenta[2,1-*b*:3,4-*b*0]dithiophene-2,6-diyl); OS, oligomeric silica; RP-17, poly(3-hexylthiophene-*co*-thiophene); βNC, β-cyclodextrin modified $CH_3NH_3PbBr_3$; P3HT, poly(3-hexylthiophene-2,5-diyl);FA-QDs, $FA_xCs_{1-x}PbBr_3$; PVP, poly(vinylpyrrolidone); P2VP, poly(2-vinylpyridine).

light and a blue laser, producing in-transfer curve shift further of and close to the initial state, respectively, as depicted in Fig. 4b and c. A fully light-controlled photomemory device (comprising n-type *N*,*N*′-bis(2-phenylethyl)perylene-3,4,9,10-bis(dicarboximide) (BPE-PTCDI) and hybrid floating gate of $CH_3NH_3PbBr_3$/poly(2-vinylpyridine) (P2VP)) has also been reported by Yang *et al.* as displayed in Fig. 4d.[36] They demonstrated in Fig. 4e–g, the full light control operations by using various visible lights (650, 530, and 405 nm) to enable photo-writing and a UV light (254 nm) in the photo-recovering process.

Subsequently, we summarized the memory characteristics of several perovskite-based floating gate photomemory transistors as tabulated in Table 1, including their device operations and conditions for a clearer comparison.

3.2. Photoactive conjugated D–A and AIE based polymer electrets

Compared to photoresponsive inorganic perovskite-based floating gates, photoactive D–A and AIE conjugated polymers provide simpler device manufacturing without additional polymer matrixes. The strong intramolecular interaction between electron-donating and electron-accepting moieties renders an exceptional charge separation ability to facilitate the dissociation of excitons into free charges.[13,14,32,65,66] Hence, the extra photogenerated charges could boost photomemory characteristics upon the dynamic operations with light. Besides, through rationale design and careful selection of the donor and acceptor groups, the energy levels of the highest occupied molecular orbital (HOMO) and lowest unoccupied molecular orbital (LUMO) of the resulting molecules/polymers can be finely tuned to match the energy alignment to favor efficient charge transfer.[67,68] Not only that, the changes of HOMO and LUMO levels could affect the photophysical properties, *i.e.*, optical band gap,[37,69] and benefitting the device operations with specific photon energy for less light interference.

While using D–A framework polymers for the photosensitive charge storage layer, Chen *et al.* designed an electret called Poly CD that comprises carbazole moiety as a donor and a dioxazine moiety as an acceptor.[13] Such attentive molecular design for the retention properties of memory devices has also been made by employing bisphenol A with a soft ether linkage instead of the fully conjugated structures that could dissipate the stored charges *via* a conductive route. Fig. 5a shows the chemical structure and device architecture in the report. The device embedded photoactive Poly CD can be electrically programmed to move the V_{th} away from the initial state and photorecovered that went *vice versa*, as shown in Fig. 5b and c. However, surprisingly, the Poly CD can also store both positive and negative charges, implying the ambipolar behavior of the charge storage electrets that could be applied to p-type or n-type semiconductor active channels. Aside from D–A conjugated polymer electrets that commonly show aggregation-caused quenching (ACQ) effect, the use of novel aggregation-induced emission (AIE) polymers as an electret layer could further switch the storage behavior of non-volatile memory from flash to write-once-read-many (WORM) by tailoring the torsion-angle between the motif of the donor and acceptor moieties (see Fig. 5d).[14] This has been recently reported by Ke *et al.* that the AIE polymer electrets could perform the photo-writing operation (by blue light, 405 nm), impacting the transfer curve shift away from the initial state, as presented in Fig. 5e and f. They claimed that the first authentic ultrafast photo-response time achieved 0.1 ms among the polymer-based transistor photomemories. Not only that, the device performed with a stunning current switch ratio of about 10^6 and retention time of over 40 000 s, which is attributed to the instantaneous recombination of the forming interlayer excitons immediately after light stimulation to the AIE polymers at the interface within the active semiconductor and AIE polymer even in the absence of applied vertical and parallel electric fields.

Table 2 summarizes some photonic transistor memory performances using D–A and AIE conjugated based polymer electrets.

3.3. Photoactive supramolecular based polymer electrets

Beyond the D–A and AIE conjugated polymers as elucidated previously, the novel supramolecular-based electrets also

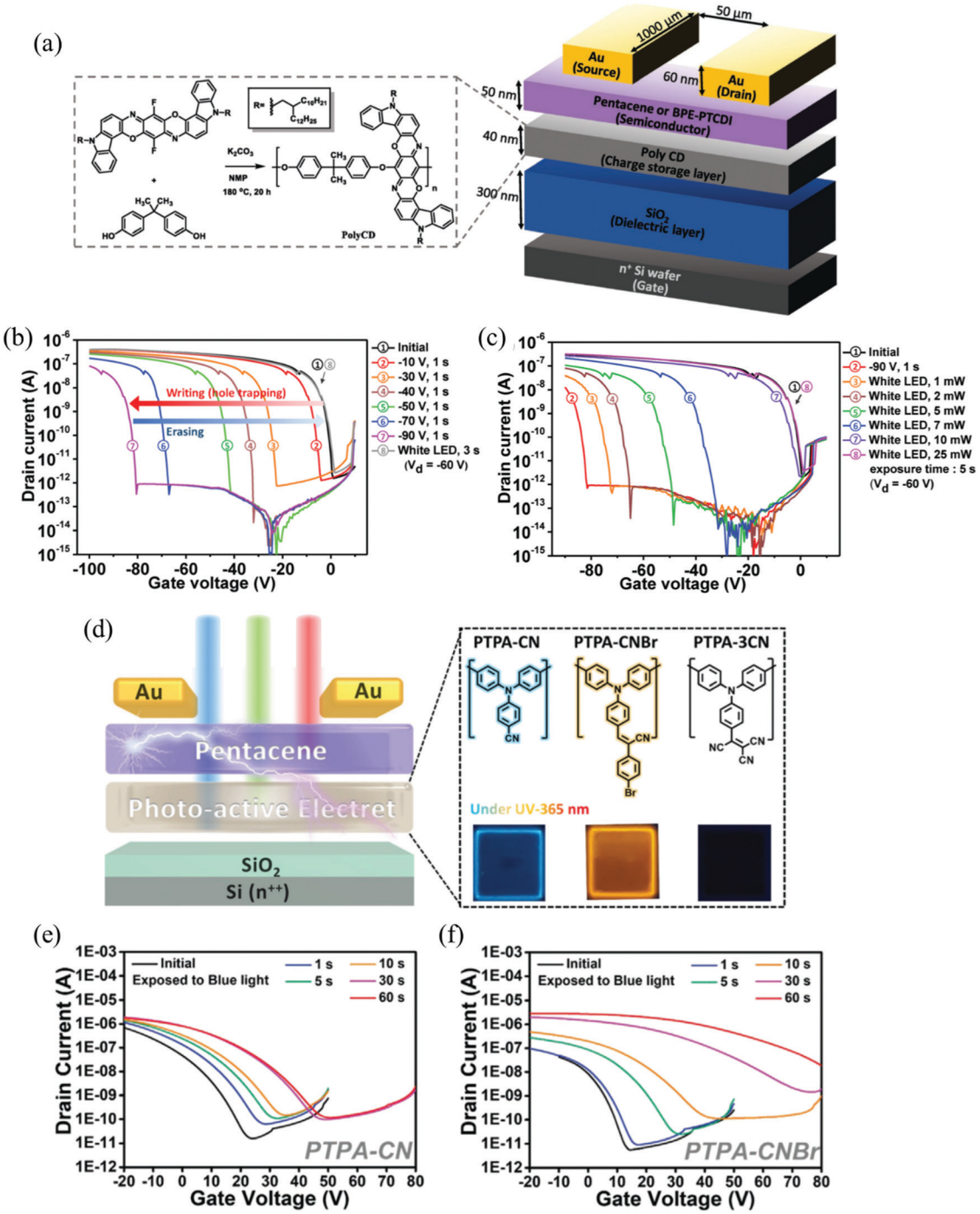

Fig. 5 (a and d) show device structures of polymer electrets based photomemories, including the chemical motifs of donor–acceptor moieties. (b, c, e and f) show the respective transfer curves after a variety of electrical programming, photo-recovery, and photo-writing processes. (a–c) Reprinted with permission from ref. 13. Copyright 2019 WILEY-VCH Verlag GmbH & Co. KGaA, Weinheim.[13] (d–f) Reprinted with permission from ref. 14. Copyright 2021 Wiley-VCH GmbH.[14]

exhibit astounding charge transfer properties through non-covalent interactions[70–72] between the self-assembly packing structure of the donor and acceptor moieties.[73] Hence, the discrete configuration of supramolecular-based electrets can ensure better stability of the trapped charges within the respective host–guest molecules.

In the early stages, the electrically operating supramolecular-based memory devices have been moderately inspected.[74–76] However, just recently, the incorporation of photoactive supramolecular electret into the memory device has been reported and it showed superior bistable memory switchability with instantaneous photo-recovery capability

Table 2 The comparison device performance of photoactive conjugated D–A and AIE polymer electrets based photonic transistor memories with the SiO_2 blocking layer

SiO_2 thickness	Photoactive charge storage material	Programming/erasing operation (V)	Programming/erasing time (s)	ΔV_{th} (V)	I_{ON}/I_{OFF} ratio	Retention time (s)	Ref.
300	PolyCD	−90/light (white LED)	1/5	82	$\sim 10^5$	10^4	13
300	Copoly(CBT)	−90/light (white LED)	1/5	49	$\sim 10^3$	10^4	65
300	PTPA-3CN	−100/light (365 nm)	1/0.5	60	$\sim 10^4$	10^4	14,32
300	PTPA-CNBr	−100/light (405 nm)	1/0.1	18	$\sim 10^6$	$>10^4$	14,32
100	PFO-*b*-$POXD_{10}$	−60/light (254 nm)	5/5	20.14	$\sim 10^5$	$>10^4$	66
300	PFO	−100/light (254/365 nm)	5/1	78	$\sim 10^7$	10^4	34

* Abbreviations: PolyCD, carbazoledioxazine polymer; copoly(CBT), carbazole/thiophenebenzothiadiazole–thiophene copolymer; PTPA-3CN, poly[4-(tricyanovinyl)phenyl]diphenylamine; PTPA-CNBr, [4-(α-cyanostilbene)phenyl]diphenylamine; PFO, poly(9,9-dioctylfluorene); POXD, poly (vinylphenyl oxadiazole).

under UV (365 nm) and green light (525 nm).[43] In this report, Yang *et al.* have intensively investigated the photoactive supramolecular electret that constitutes of poly(1-pyrenemethyl methacrylate) (PPyMA) host polymer and 7,7,8,8-tetracyanoquinodimethane (TCNQ) guest molecule. Fig. 6a shows the host polymer and the guest molecule structure and the device layout of the supramolecular electret-based photonic memory transistor. The modulated transfer curves displayed in Fig. 6b–e behave distinctively with different contents of TCNQ molecules under V_g bias of −50 V for 1s (resulting in more negative V_{th}) and various photorecovery durations (resulting in the V_{th} shifts to the positive direction) with UV light. It showed that with an equivalent molar content of pyrene (as a functional moiety in the host polymer) and TCNQ (as a guest molecule), the associated device (PPyT-2) performed exquisitely along with a wide memory window (ΔV_{th} = 34 V), large memory ratio of about 3.1×10^6, long retention capability over 10^4 s, and robust memory endurance (WRER cycles over 100).

To clarify the supramolecular-based transistor memory performances, both electrically controlled and partially photo-driven devices are recapitulated in Table 3.

4. Physical device mechanism in association with the device operations

In this section, the physical mechanism of photonic transistor memories will be elucidated in more detail according to the V_{th} shift response upon the device operations as observed in the previous section. Then, in general, as illustrated in Fig. 7, the working principles of photomemory transistors could be divided into several categories as follows:

4.1. Photo-writing mechanism

Photo-writing phenomenon can be observed when the transfer curve shifts away from the initial state after the excitation of the photoresponsive charge storage layer with light exposure, resulting in high throughput I_d in the reading mode. As was exemplified in the previous section, often, the perovskite-based floating gate photonic memory device unveils this phenomenon. Thus, to elucidate the plausible process mechanism for the photo-writing operation, we brought the arguments from Chen's report[24] involving a simple system based on perovskite/insulating polymer blend floating gate photonic memory, as displayed in Fig. 3a. In general, the photophysical properties and frontier molecular orbital energy levels (HOMO and LUMO) of both, the active layer and photoactive material, are essential to be clarified, as the photoinduced generation of free charges, charge transfer behavior, charge polarities, as well as, charge trapping abilities will be strictly correlated to the memory behavior upon the device operations. Fig. 8a shows the absorption spectra of the $MAPbBr_3$/PS composite film in comparison to the pentacene film. As can be expected, the $MAPbBr_3$/PS composite film possesses distinct absorption regions against the pentacene film, which makes it less absorbing interference. Moreover, the PL spectra in Fig. 8b confirms the efficient photoexcitons' dissociation and charge transfer in between the $MAPbBr_3$/PS composite film on pentacene, which is demonstrated by a rapid PL quenching compared to the controlled $MAPbBr_3$/PS composite film on quartz. Following this scheme, the corresponding schematic band diagrams of pentacene, perovskite $MAPbBr_3$, and PS materials can be drawn, as shown in Fig. 8c to explain the process mechanism. Upon the photo-writing, the incident light source with photon energy closely matching the perovskite band gap energy will be absorbed properly and in turn generate more hot photoinduced carriers within the confined perovskite nanoparticles. Owing to the low conduction band of the perovskite material, the photoinduced electrons will remain and be stabilized in the perovskite, whilst the photogenerated holes will likely tunnel through the PS matrix and transfer to the HOMO level of pentacene. It is worth noting that the spatially discrete distribution of perovskite nanoparticles in the PS matrix can effectively suppress the charge trapping dissipation.[24] Subsequently, this situation creates an internal built-in electric field that provides the hole accumulation region, furnishing the unchanged state of the photonic memory device. On the other hand, the charged device due to the trapped electrons in perovskite nanoparticles can be neutralized by applying the negative V_g bias that will draw the holes from the HOMO level of pentacene and overcome the potential barrier of the PS matrix and then recombine non-radiatively with the trapped electrons.

There also occurred a photo-writing behavior of the photonic memory devices based on AIE polymer electret as

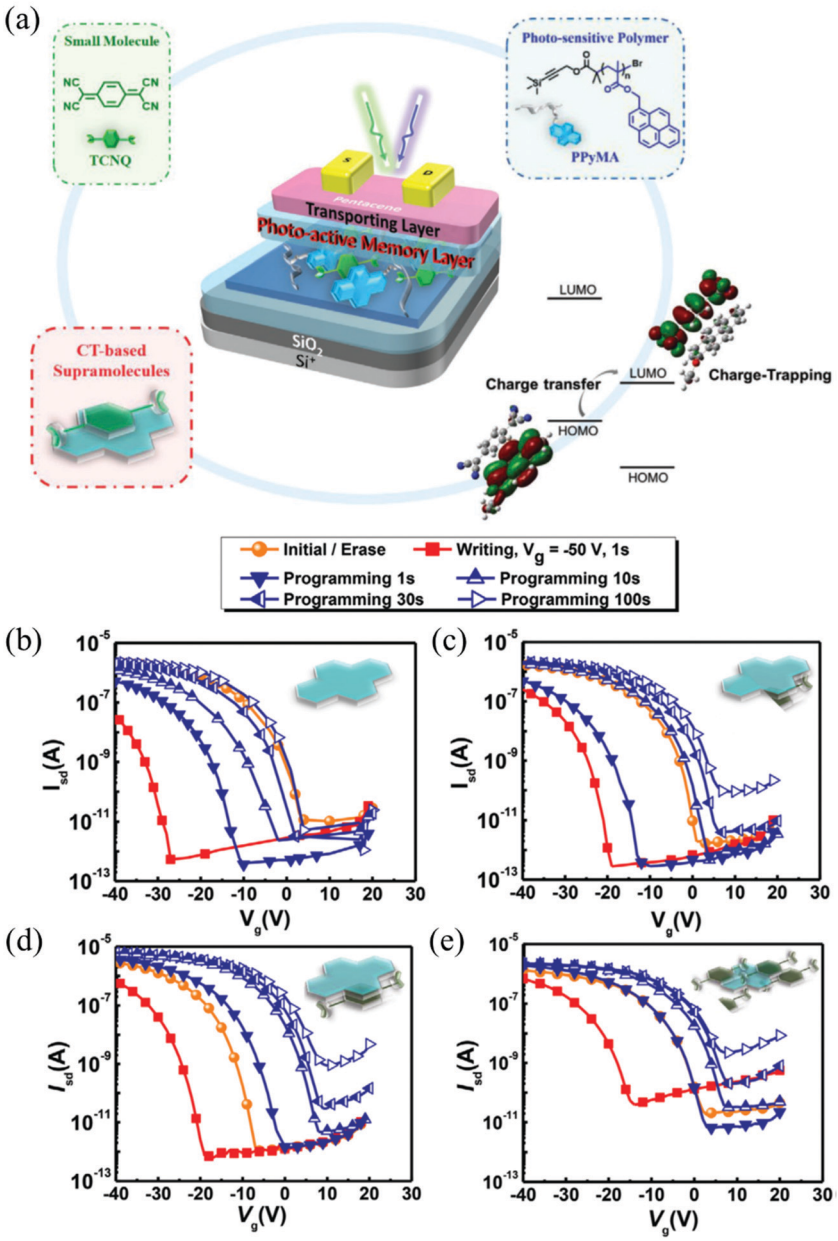

Fig. 6 (a) The device structure and chemical motifs of the host polymer and guest molecules in supramolecular electret-based photomemory. (b–e) Transfer curves of the respective devices with various concentrations of guest molecules. Reprinted with permission from ref. 43. Copyright 2021 Wiley-VCH GmbH.[43]

Table 3 The comparison device performance of photoactive supramolecular polymer electrets based photonic transistor memories with the SiO_2 blocking layer

SiO_2 thickness	Photoactive charge storage material	Programming/erasing operation (V)	Programming/erasing time (s)	ΔV_{th} (V)	I_{ON}/I_{OFF} ratio	Retention time (s)	Ref.
300	P4VP(2-naphthol)	100/−100	1/1	61	$>10^7$	10^4	75
100	AM4/PI	40/−40	1/1	29.95	$>10^4$	10^4	76
100	PPyT-2	−50/light (365 nm)	1/100	34	$>10^6$	10^4	43

* Abbreviations: P4VP, poly(4-vinylpyridine); AM4, 1-aminopyrene; PI, polyimide; PPyT-2, poly(1-pyrenemethyl methacrylate) + 50 mol% 7,7,8,8-tetracyanoquinodimethane (TCNQ).

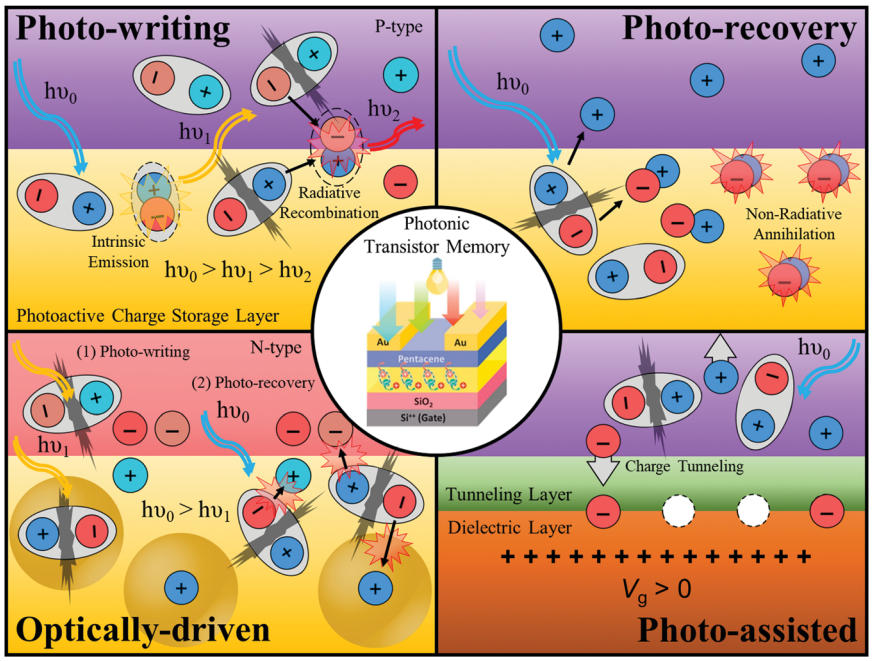

Fig. 7 A representation of the device operations along with its process mechanisms that are applied in the photonic memory transistor devices.

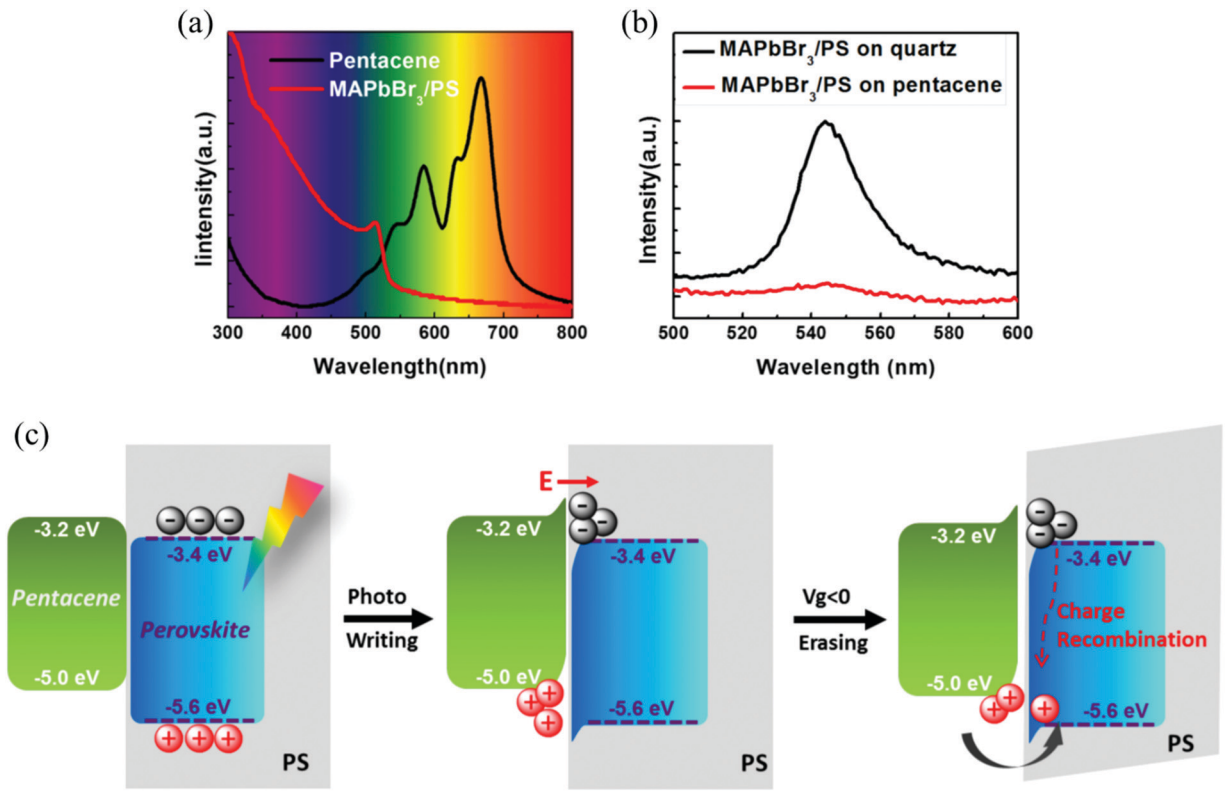

Fig. 8 (a) Optical absorption spectra of the pentacene film and MAPbBr3/PS composite film. (b) PL characteristics of the MAPbBr3/PS composite film on quartz and on pentacene with light excitation at 450 nm. (c) Photo-writing and electrical erasing process mechanisms. Reprinted with permission from ref. 24. Copyright 2017 WILEY-VCH Verlag GmbH & Co. KGaA, Weinheim.[24]

mentioned earlier, as shown in Fig. 5d–f. Even though, it offers a simpler device preparation and less sophisticated system (solely a polymer electret in contrast to the floating gate system with two distinct materials), even so, the proposed plausible device mechanism is quite fascinating and implicates the interlayer excitons at semiconductor/AIE polymer electret

interface.[14] Fig. 9a depicts the emission spectra of bilayer films of pentacene/AIE polymer electret (with an excitation wavelength of 405 nm) with the appearance of a new emission band of the interlayer excitons. It is elucidated from the schematic band diagrams portrayed in Fig. 9b. Owing to the difference in the HOMO levels for both AIE polymers and pentacene being higher than 0.15 eV, which is in the range of the binding energy of Frenkel excitons,[77,78] the radiative relaxation pathway could be preferred. Hence, the noticeable new emission band in bilayer films could be attributed to the interlayer-recombined exciton from the LUMO level of pentacene and the HOMO level of AIE polymer.[79–81] The photo-writing mechanism then could be elaborated, as illustrated in Fig. 9c. The photoactive AIE polymer-based electret layer firstly generates excitons upon exposure to blue light. Then, a fraction number of excitons established within the electret layer would self-recombine and hence emit its intrinsic emission spectrum. The emitted photons from the electret layer could effectively be absorbed by pentacene to produce its own excitons simultaneously, and eventually, each type of opposite photoinduced charge migrate to their suitable energy levels, where electrons reside in the electret layer and holes remain in pentacene. In this state, the transfer curve and V_{th} position of the device will shift away to the positive region, impacting the normally high output I_d.

4.2. Photo-recovery mechanism

Whereas the exact opposite of photo-writing, that is the photo-recovery phenomenon, the noticeable event occurs conversely. This implies that, the transfer curve of the device after receiving an appropriate light source by the photoactive charge storage layer, will lead to the displacement towards the initial condition. Indeed, the phenomenon will take place prior to the charging operation of the device (the transfer curve must be quite distant from the initial state after V_g bias programming). On numerous occasions, this phenomenon appears on the photonic memory devices employing photoactive polymer electrets, *e.g.*, D–A and AIE conjugated polymers that have been presented in the previous section. Although some reports believe that the photo-recovery occurrence could be caused by the recombination of trapped charges with the photoexcitons from the semiconducting layer (*i.e.*, pentacene),[82] yet, other reports state that the photoactive electrets have a significant role in generating excitons that *in situ* instantaneously neutralizing the trapped charges within it.[13,65] To confirm this aspect, Chen *et al.* reported such a straightforward demonstration.[34] They directly engaged the photo-recovery operation between commercial photoactive polymer polyfluorene (PFO) electret and non-photoactive insulating poly(vinyl alcohol) (PVA) polymer under the same device configuration, as depicted in Fig. 10a.

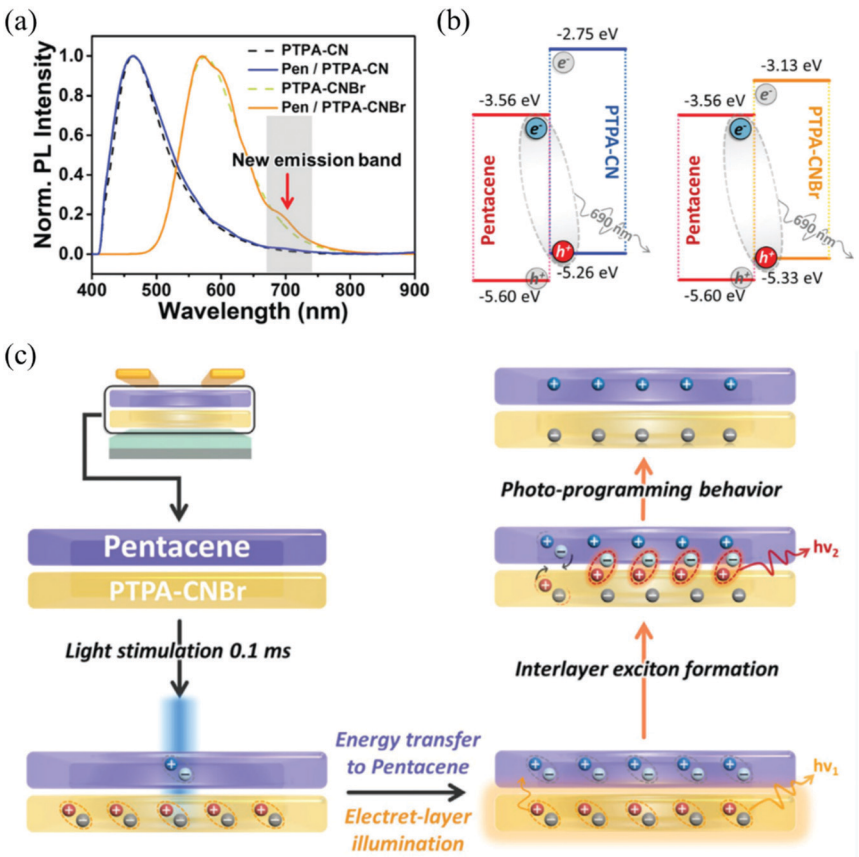

Fig. 9 (a) Device structure of perovskite based floating photomemory, in line with the well-distributed perovskite nanoparticles within the polymer matrix. (b) Photo-writing and electrical erasing process mechanisms. Reprinted with permission from ref. 14. Copyright 2017 WILEY-VCH Verlag GmbH & Co. KGaA, Weinheim.[14]

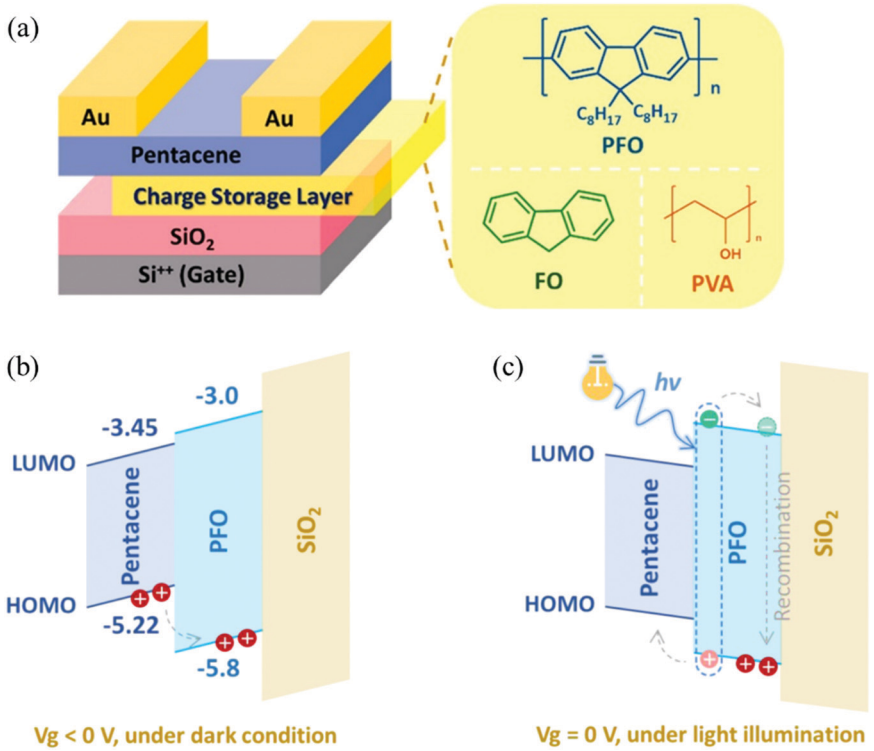

Fig. 10 (a) Photomemory transistor structure with photoactive polymer electrets. (b) Electrical-programming and (c) photo-recovery mechanisms explained with schematic band diagrams. Reprinted with permission from ref. 34. Copyright 2021 American Chemical Society.[34]

The aftermath showed that the device without photoinduced excitons' ability (a device that employed PVA as an electret) was unable to exhibit a remarkable photo-recovery phenomenon. Although the light source exposed to the device can also excite the pentacene semiconductor layer, the study showed no conspicuous photo-recovery, as compared to PFO photonic transistor memory. Concisely, the photoresponsive polymer electret literally governs the *in situ* neutralization of the charged device. The photorecovery mechanism was then could be unveiled, as illustrated in Fig. 10c. In the beginning (see Fig. 10b), the device is electrically charged by exerting V_g at a negative bias to enable the hole trapping process in the polymer electret layer. Subsequently, a decent illumination of light on the photoactive polymer electret renders the photogeneration of electron–hole pairs that dissociate into electrons to *in situ* neutralize the trapped holes and the photoinduced holes that will be escaping to the HOMO level of pentacene. As a result, the eliminated trapped holes in the electret dispel the built-in electric field, yielding a neutral device with low output I_d and/or recovering the device to its initial condition.

4.3. Optically-driven mechanism

The fully optical controlled photonic memory transistor is an exceptional memory device. The device structure and memory behavior have been thoroughly described in the previous section shown in Fig. 4d–g. Such a device most likely has a photoactive charge storage layer containing two distinct photoactive materials that possess low band gap perovskite nanoparticles and a wide band gap P2VP polymer matrix (see Fig. 11a and b).[36] Hence, the adoption of a floating gate type of charge storage layer into the device is the most suitable one for this application. On this account, the photoactive floating gate layer could be able to perform photo-writing and photo-recovery by using different photon energies (light wavelengths). As displayed in Fig. 11c and d, the device mechanism can be interpreted as follows: in the photo-writing step, first, the use of visible light (low photon energy; 405–650 nm) will produce photoexcitons in perovskite nanoparticles and/or BPE-PTCDI (depending on the absorption property of these two materials) and subsequently dissociated into photoinduced electrons and holes. Based on the favorable band energy matching illustrated in the schematic diagram, the electrons will migrate from the perovskite to BPE-PTCDI, whilst the holes are transferred oppositely. In this situation, the floating gate will preserve the holes that are possibly trapped at the perovskite/P2VP interface, and otherwise the electrons retained in BPE-PTCDI. The positively charged floating gate layer then induces a more electron accumulation region at the bottom interface of BPE-PTCDI, inflicting the high output I_d of the device. On the contrary, the application of high photon energy (UV light; 254 nm) will perform the photo-recovery process on the device. Since the P2VP polymer matrix possesses a much wider band gap compared to perovskite and BPE-PTCDI materials, the UV light will be intensely absorbed and generate the photoexcitons, followed by excitons' dissociation into free charge carriers.

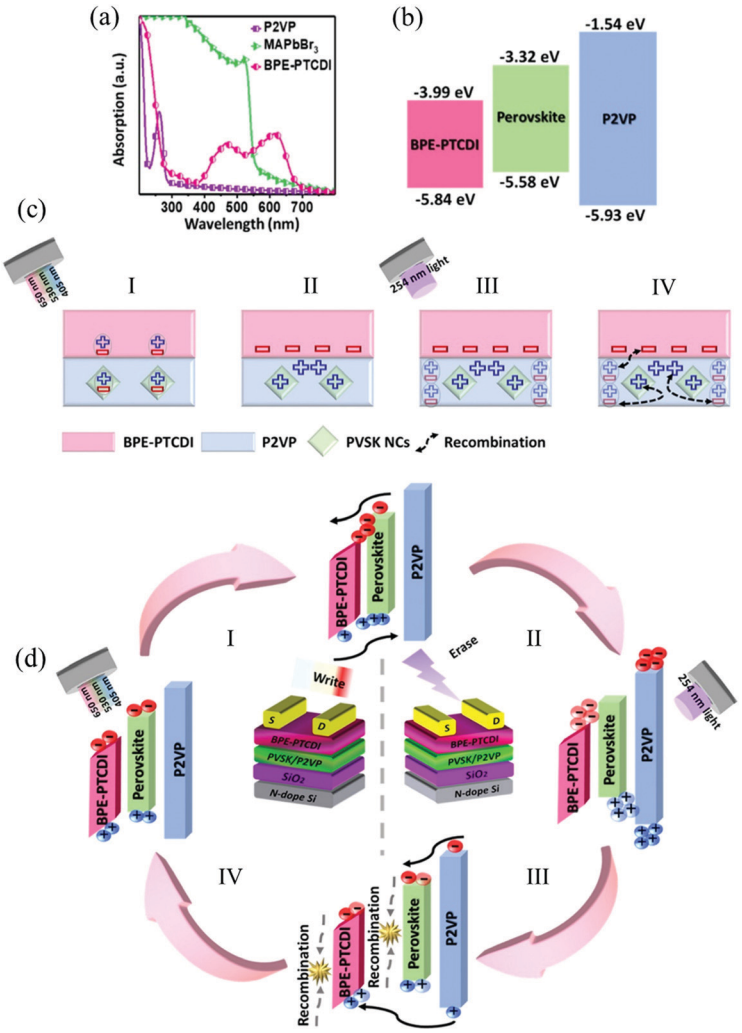

Fig. 11 (a) Absorption spectra of n-type BPE-PTCDI, perovskite MAPbBr3, and polymer matrix P2VP. (b) The respective energy bands. (c) Charge migration upon photo-writing (charging electret) and photo-recovery (neutralizing electret) processes on the fully optical driven photonic memory transistor. (d) Schematic energy band diagrams in association with the photo-writing and photo-recovery processes. Reprinted with permission from ref. 36. Copyright 2021 American Chemical Society.[36]

The photoinduced free charge carriers within P2VP eventually migrate to the adjacent perovskite nanoparticles and BPE-PTCDI, thus, neutralizing the respective trapped charges as well as the device.

4.4. Photo-assisted mechanism

From the device operation and mechanism, as listed above, it has been reported that the transistor memory devices could have an extra elevated memory performance when the light and V_g bias are exerted simultaneously. This operation, namely, "photo-assisted" programming or erasing has been intriguingly demonstrated in the literature.[39,58,83–86] Several memory devices found in the literature that underwent these operations are tabulated in Table 4. However, what is more astonishing is that the regular transistor device without the photoactive material or charge storage layer could exhibit an outstanding memory characteristic. For the representative case, as shown in Fig. 12, a widely-used conventional OFET that constitutes a pentacene semiconducting channel on a silicon wafer with the octadecyltrimethoxysilane (OTS)-modified SiO_2 layer can operate reversibly between the normal transistor and memory transistor devices flawlessly.[8] Following this peculiar case, the authors highlighted that the photogenerated excitons and tunneling effect played a significant role in manifesting the photomemory behavior. In short, the photogenerated excitons stem from the semiconductor active channel upon illumination, whilst, the tunneling effect occurs at the same time when a sufficiently large electric field exists, driving the respective free charges (in the semiconducting channel) to overcome the tunneling barrier potential and get trapped (see Fig. 12). In the figure, photo-assisted programming (light exposure and a positive V_g bias) causes the separated free electrons to tunnel through a thin barrier of the OTS layer and fill up the intrinsic interface traps of the SiO_2 layer. As a result, the trapped

Table 4 A comparison of device performance of regular/memory transistor with the SiO_2 blocking layer under photo-assisted programming and/or erasing

SiO_2 thickness	Photoactive charge storage material	Programming/erasing operation (V)	Programming/erasing time (s)	ΔV_{th} (V)	I_{ON}/I_{OFF} ratio	Retention time (s)	Ref.
200 nm	Au/PS nano-floating-gate	Light + 80/light + (−80)	1	120	$\sim 10^4$	10^3	39
100 nm	6FDA-DBA-SP	Light + 40/−40	10/1	—	$\sim 10^4$	$>10^4$	84
300 nm	Au/Porous PMMA	Light + 80/−150	3	43	$\sim 10^4$	10^4	58
—	Charge storage layer FREE	Light + 120/−120	10	59.7	$\sim 10^6$	$>10^4$	85
300 nm	Ag/PMMA	Light + 10/light + (−10)	1	1.67	—	10^5	86
300 nm	Charge storage layer FREE	Light + 100/−100	10	50.1	$\sim 10^6$	10^4	8

* Abbreviations: PS, polystyrene; 6FDA-DBA-SP, poly(3,5-benzoic acid hexafluoroisopropylidene diphthalimide); PMMA, polymethylmethacrylate.

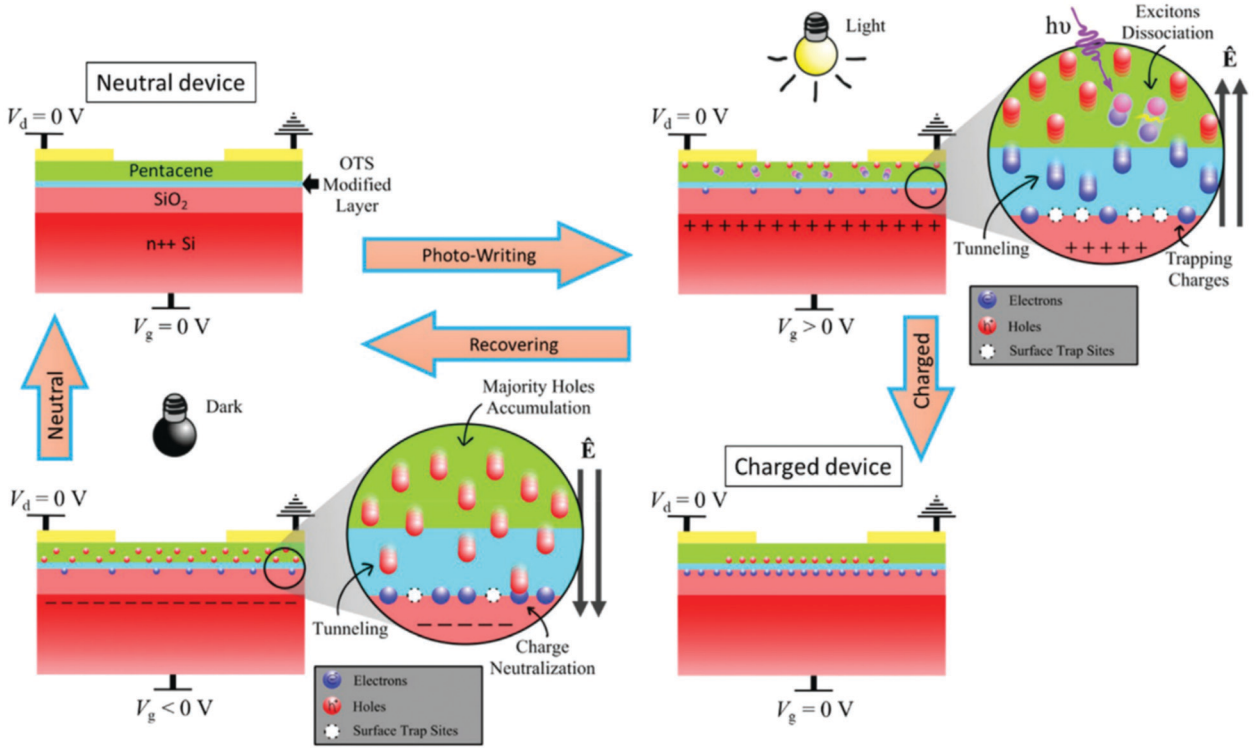

Fig. 12 The mechanism process of photo-assisted programming and electrical erasing *via* tunnelling-effect of the photonic memory transistor device. Reprinted with permission from ref. 8. Copyright 2022 Wiley-VCH GmbH.[8]

electrons would induce the hole accumulation region and transform the device with a normally high output I_d. Henceforth, owing to the tunneling effect, when a large negative bias is applied during the erasing process, the majority of holes at the bottom interface of the pentacene layer can be drawn, overcoming the barrier potential, neutralizing the trapped electrons, and transforming the device into the neutral state. To this end, the concise and understandable mechanism with the above-mentioned straightforward results render the tunneling-effect in the photo-assisted transistor memory, as to be a new branch of research in this field that needs more attention. Besides, the concept is practically applicable to new photoactive semiconductors,[33,44,87] novel photo-functionalized tunneling barrier materials,[49,50,88] or even for the inherent rich surface traps of high-k dielectrics,[89,90] which will provide more options for the improvement.

5. Potential applications benefitted from transistor photomemory devices

As mentioned in the introduction section, many promising applications in the rapid growth of IoT[4] and AI[5,6] have been realized by adopting the concept of device operations and mechanisms of transistor photomemory.[7–17] Among the plethora of applications, in this section, the discussion will focus on two crucial applications, there are multilevel storage memory cells[7,8] and artificial synapses[10,11] due to the similarity

of working principle utilization;[91] for other fascinating and feasible applications based on photonic memory devices can be found in the recent reports and literature reviews.[20,30,44,50,92–97]

5.1. Multilevel photomemory for high-density storage

The increased usage of data information in this era will likely burden the current storage technology, which keeps the data in a one-bit memory cell.[98,99] Conventionally, increasing the density of memory cells to enlarge the storage capacity can be attained by scaling down a cell of memory devices. In doing so, albeit, this technique will soon face the difficulties owing to the physical and technical limitations. On the other hand, such a breakthrough concept to store multibit per cell of memory devices may solve the addressed issue and can be practically employed in the current technology.[19,24,83,100–109] To achieve this purpose, a photonic memory device could generate distinguishable memory states in between the highest and lowest drain output current by precisely controlling the charge injection or the elimination rate under various device operations (gate bias strength, light intensity, and/or bias/exposure times) as discussed previously. In this regard, the number of trapped charges within the trapping sites will be responsible for the varied built-in potentials as well as the magnitude of the drain output current in a non-volatile way.

For example, besides low power consumption and fast photomemory modulation, an article has reported an unprecedented photonic memory cell that could possess over 256 (8-bit storage) distinct current levels.[100] The strategy was devised using the active channel blend of a common high-performance polymer semiconductor poly(3-hexylthiophene) and a photochromic diarylethene which can be switched under UV (closed isomer; appropriate energy levels for charge transfer) and green (opened isomer; inappropriate energy levels) light irradiation to control the rate of charge injection. The resulted memory device showed highly robust over 70 write-erase cycles, including the retained memory state over 500 days. In the recent report, the monitoring device for deep ultraviolet (DUV) light-sensing based on non-volatile photoelectric memory of OFET has demonstrated 16 distinct optical memory states (4-bit storage) and rewriting capability, indicating the superior multilevel memory behavior.[110] Consisting of diketopyrrolopyrrole-dithienylthieno[3,2-*b*]thiophene (DPP-DTT) as an active channel, and poly(perfluoroalkenylvinyl ether) (CYTOP) on SiO_2 substrate built-up the DUV photoelectric memory device along with retention of over 10^4 s, and more than 100 cycles of WRER operations. In the following progress, a transistor photomemory incorporating a ferroelectric (insulating) layer of poly(vinylidene fluoride-trifluoroethylene) (PVDF-TrFE) could offer several advantages compared to the conventional organic insulators[111] by virtue of its relatively large fatigue-free remnant polarization,[112] faster switching time, and better thermal stability.[19,113,114] The yielded memory device is capable of operating in 11-bit storage per memory cell along with precise control of readout drain current and feasible repeatability, and even instant (milliseconds) and low light intensity (<1 μJ cm^{-2} s^{-1}) of optical writing process.[19]

5.2. Photosynaptic transistor for visual perception

Meanwhile, the working principles, device operations, and capabilities of transistor photomemory have also been utilized in mimicking and emulating the complex biological functions such as nerve signal transmission to neuromorphic computing applications, and even recreating image memory for new-generation visual prosthetics and artificial visual perception systems such as a human eye (for example see in Fig. 13a).[91,115–126] The so-called ''photosynaptic transistor'' resembles that of a biological synapse construction wherein the source/drain terminals can be associated with the pre-/postsynapses, and the external light stimuli/gate bias corresponds to the action potentials exerted in the presynapse (see Fig. 13b). The neurotransmitters within a synapse system could be represented as the charge carriers dwelling in the semiconducting layer within the source/drain circumference. In regard to this, the device mechanisms are quite similar, frankly speaking, the same to the mentioned physical working principles in the fourth section. Taken as an example from Fig. 13c, the respective band energies are drawn schematically based on the mixed quantum dot photoabsorbers and metal-oxide semiconducting layer that built-up a photosynaptic transistor in a recent report.[115] Upon the incident light signal pulse to the device (an action potential exerted presynapse), the photogenerated electron–hole pairs in quantum dots (photoactive materials, in general) are readily separated, and subsequently, the electrons transfer to the most favorable energy level which is in the metal-oxide part. On the other hand, the holes are effectively confined in quantum dots because of an unfavorably high potential barrier.[115] This mechanism is kind of similar to the photo-writing phenomenon for a transistor photomemory elaborated in the fourth section.

Moreover, there are several key factors to be considered the synaptic behavior in photosynaptic devices, as follows: the excitatory postsynaptic current (EPSC) or inhibitory postsynaptic current (IPSC), which indicates an escalation (carrier capture) or depletion (carrier release) of the readout current in gauging the neuron connection (synaptic strength or weight); short-term plasticity/memory (STP/STM) and long-term plasticity/memory (LTP/LTM), indicate the flexibility to adjust the learning and recollection memory processes similar to the human brain. The STM characteristic itself could be indicated under the application of paired-pulse facilitation (PPF) or paired-pulse depression (PPD), which results in an increase or decrease in the ratio of postsynaptic current amplitude within the two successive spikes (see Fig. 13d). Whereas, the LTM relates to the slow decay of EPSCs as the synaptic weight increases with pulse width, the number of pulses, and its interval in attaining the spike number-dependent plasticity (SNDP), spike-time-dependent plasticity (STDP), and spike rate-dependent plasticity (SRDP). The entire factors above, in common, can be modulated by gate/drain bias or light intensity, wavelength, and exposure time in pulsing mode with different amplitudes/widths/frequencies/numbers to emulate both STM and LTM in the human brain, as exemplified in Fig. 13e to g. And most importantly, the energy consumption of

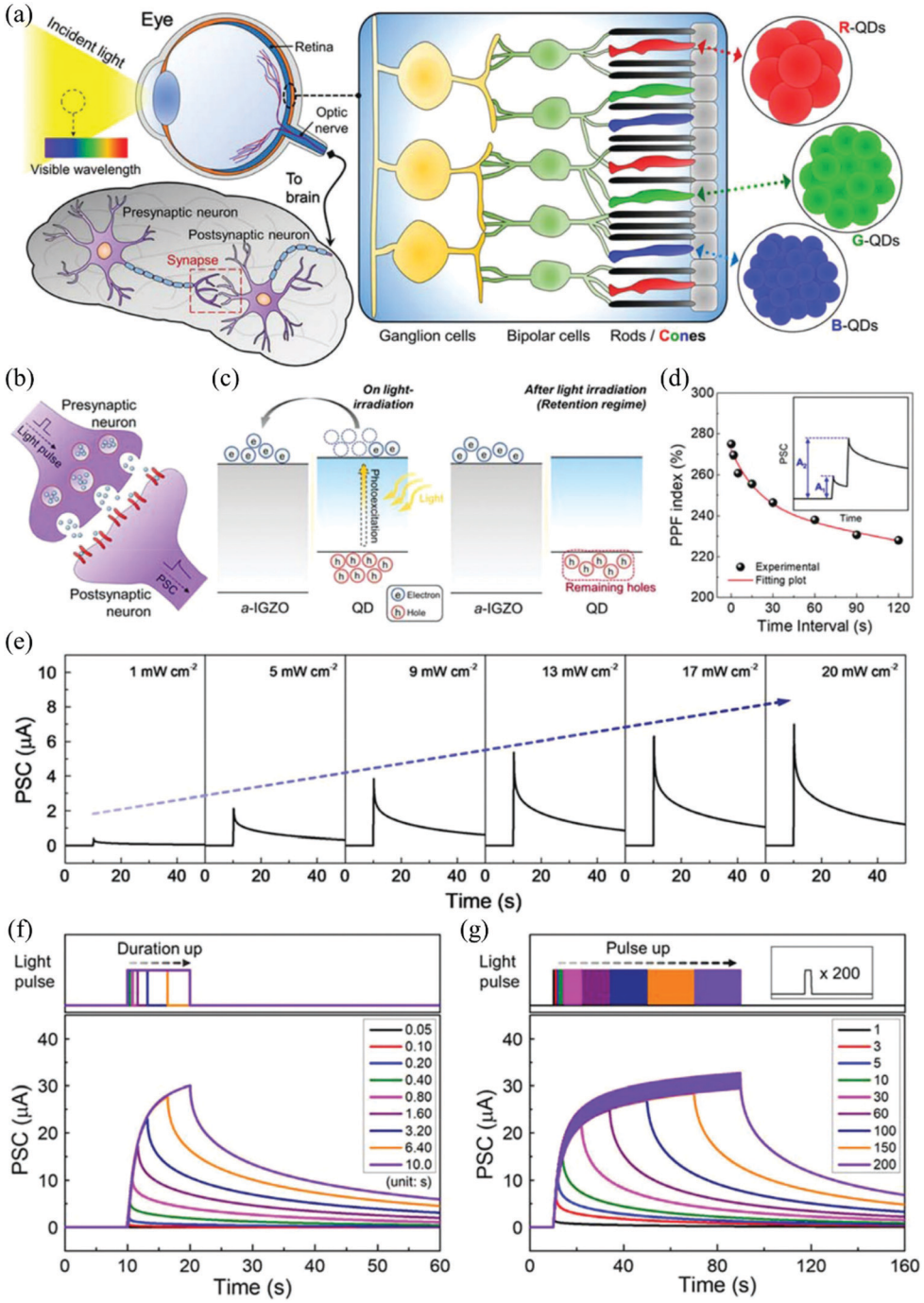

Fig. 13 (a) An illustration of the human visual system in the human brain containing neurons and synapses. (b) An analogy of the biological synapse process. (c) Process mechanism in the energy band diagram. Photosynaptic behavior under light pulse stimuli: (d) pulse interval-dependent PPF index triggered by two spikes, (e) pulse intensity-dependent postsynaptic current (PSC), (f) pulse duration-dependent PSC, (g) pulse number-dependent PSC. Reprinted with permission from ref. 115. Copyright 2022 Wiley-VCH GmbH.[115]

photosynaptic transistor could be a great consideration,[127] on account of emulating ultralow energy consumption per synaptic event (*ca.* 1–100 fJ) in the human brain.[125,128,129] The energy consumption (E_{on}) can be estimated as $E_{on} = I_{peak} \times t \times V$, where I_{peak}, t, and V are the maximum peak value of the EPSC or IPSC, pulse duration time, and applied pulse voltage, respectively.[60] Knowing these parameters for the photosynaptic transistor-based device is essential. In the latter paragraph, the progress of photosynaptic transistors will be elaborated on the latest reports found in the literature which are not limited to the use of photoactive organics/polymers,[97,130,131] but also hybrid-inorganics and other potential photoactive materials.[115,118,119,121,132]

In our recent work on photosynaptic transistors, the use of single-walled carbon nanotubes (SWCNTs) wrapped single-layered poly(9,9-dioctylfluorene)-*b*-polyisoprene (PF-*b*-PI) which serves as both semiconductor and electret layer has demonstrated.[11] Owing to the high charge carrier mobility of SWCNTs ($\sim$11.3 cm^2 V^{-1} s^{-1}) and inherently photoactive conjugated polymer of PF-*b*-PI, this hybrid material endows the device with high output current (10^{-4} to 10^{-3} A) and finely-modulated synaptic behavior against either light or electrical signal. Besides possessing a large memory window ($>$70 V), the LTP to LTD could be emulated under 21 light pulses of blue light (395–415 nm at 25 mW cm^{-2}) for 10 s each at the intervals of 30 s and continually monitoring the PSC in the dark for 1000 s, and the synaptic PPF behavior by the application of pair of presynaptic light pulses for 10 s each at intervals of 300 s. The electrical triggered synaptic properties resulted in the PPF index (a time interval of the synaptic device, which follows a biexponential function to identify and decode information)[20] that matches well with the biological counterpart. In addition to that, the higher EPSC triggered by the second spike is usually ascribed to the charges accumulated from the earlier spike that is not able to fully dissipate, inflicting the more trapped charges for the incoming spike.[133] As for the perovskite-based photosynaptic transistors, the reported devices could consume ultralow energy per synaptic event (0.03–0.18 fJ)[60,132] as close as in the human brain. Those were rationally and carefully designed, such as by investigating the influence of A-site substitution[60] and the solution processing and pretreatment with ultrasonication and UV irradiation.[132] On top of that, by introducing an ultra-thin charge carrier regulator layer that is hexagonal boron nitride (h-BN) sandwiched between perovskite quantum dots and graphene, such a device can impart improved the PPF index (up to $\sim$196%) which is required in realizing high-precision artificial visual perception system.[121] Last but not least, the development of polymer-based photosynaptic transistors keeps pace with other potential materials.[122,130,131,134] In this scope, a photosynaptic transistor utilizing P3HT-*b*-P2VP block copolymer active layer could emulate PPF, STDP/SRDP, and STP/LTP behaviors.[130] The corresponding LTM can keep the current contrast to 10^5, the STM with a high PPF ratio of 1.38, and an ultralow energy consumption calculated *ca.* 0.56 fJ at an application voltage of –0.0003 V stimulated under blue light (450 nm, 2.2 mW cm^{-2}, for 0.2 s). A simpler polymer-based photosynaptic device with capabilities to simulate various synapse-like behaviors such as EPSC, PPF, STM/LTM and its transition using DUV light was demonstrated.[131] The device contains of P3HT as active channel and CYTOP as a modifying layer for the dielectric surface with ΔEPSC values recorded up to 6.2 nA under the exertion of a single light pulse intensity of 0.15 mW cm^{-2} and duration of 4 s. And the very recent progress on photosynaptic device that using the same concept of photo-assisted operations (see in subsection of 4.4), while investigating the effect of molecular weight (Mw) of polymer electret to the photosynaptic behavior have been reported.[134] With poly(N-vinylcarbazole) (PVK) as the case study, such device could exhibit a larger memory window (28.2 V) bundling with an instantaneous programming speed of 1 ms for lower Mw PVK electret. The photosynaptic behaviors such as EPSC/IPSC, PPF/PPD, excellent tunability between STP and LTP, including high accuracy and STP-based RGB color recognition ability that could be further emulated on lower Mw PVK device by photo-assisted operations.

6. Summary and perspectives

To conclude, we have systematically presented the transistor memory device structures, basic device operations, and several important parameters used to take the measure the good performance of the memory devices. Furthermore, the novel photonic memory transistors equipped with various proposed new photoactive materials in the charge storage layer could have more versatile potential applications and facile manufacturing methods to fit in with current technological advancements. On top of that, the photomemory behavior could be delicately tuned in response to the device operations and working principles such as photo-writing, photo-recovery, and fully optically driven, depending on the rational design and material selection of the photoactive charge storage layer. All of which, benefitting from the photogenerated excitons of photoresponsive materials, the photonic memory transistor devices could offer more control on memory behavior, including low noise interference, high information security and energy consumption, and high-speed information transfer compared to ordinary fully electrically-controlled one.

In addition, the new concept of photo-assisted programming and erasing, principally shows the distinction in device operations and working mechanisms to the mentioned photonic memory transistors. Taking the advantages from intrinsic interface traps of the dielectric layer as well as the tunneling layer to stabilize charge trapping, the switchable conventional to photomemory transistor could be a general strategy for creating multifunctional photonic memory devices. Besides, the method operations have successfully demonstrated in the charge storage layer free transistors to behave as a photomemory device, hence, guaranteeing a cost-effective and facile device fabrication, for more practical and high-performance device applications.

Author contributions

Y.-C. C. contributed to supervision. S. P. P. contributed to writing – the original draft. S. P. P. and Y.-C. C. were further contributed to conceptualization and writing – review and editing. M.-N. C. was contributed to visualization.

Conflicts of interest

There are no conflicts of interest to declare.

Acknowledgements

The authors thankfully acknowledge the financial supports from the Ministry of Science and Technology in Taiwan (MOST 109-2622-E-011-030, and MOST 110-2221-E-011-009).

References

1 K. K. N. Simon and M. Sze, *Physics of Semiconductor Devices*, John Wiley & Sons, 3 edn, 2006.
2 J. S. Park, W.-J. Maeng, H.-S. Kim and J.-S. Park, *Thin Solid Films*, 2012, **520**, 1679–1693.
3 Y. Guo, G. Yu and Y. Liu, *Adv. Mater.*, 2010, **22**, 4427–4447.
4 W. Shi, Y. Guo and Y. Liu, *Adv. Mater.*, 2020, **32**, 1901493.
5 C. Wan, P. Cai, M. Wang, Y. Qian, W. Huang and X. Chen, *Adv. Mater.*, 2020, **32**, 1902434.
6 Y. Zang, F. Zhang, C.-A. Di and D. Zhu, *Mater. Horiz.*, 2015, **2**, 140–156.
7 C.-C. Shih, Y.-C. Chiang, H.-C. Hsieh, Y.-C. Lin and W.-C. Chen, *ACS Appl. Mater. Interfaces*, 2019, **11**, 42429–42437.
8 Z.-Y. Wei, S. P. Prakoso, Y.-T. Li and Y.-C. Chiu, *Adv. Electron. Mater.*, 2022, 2101349.
9 Z. He, J. Han, X. Du, L. Cao, J. Wang, C. Zheng, H. Lin and S. Tao, *Adv. Funct. Mater.*, 2021, **31**, 2103988.
10 T. Ahmed, M. Tahir, M. X. Low, Y. Ren, S. A. Tawfik, E. L. H. Mayes, S. Kuriakose, S. Nawaz, M. J. S. Spencer, H. Chen, M. Bhaskaran, S. Sriram and S. Walia, *Adv. Mater.*, 2021, **33**, 2004207.
11 M. M. Mburu, K.-T. Lu, N. L. Prine, A.-N. Au-Duong, W.-H. Chiang, X. Gu and Y.-C. Chiu, *Adv. Mater. Technol.*, 2022, 2101506.
12 C.-C. Hung, Y.-C. Chiang, Y.-C. Lin, Y.-C. Chiu and W.-C. Chen, *Adv. Sci.*, 2021, **8**, 2100742.
13 C.-H. Chen, Y. Wang, H. Tatsumi, T. Michinobu, S.-W. Chang, Y.-C. Chiu and G.-S. Liou, *Adv. Funct. Mater.*, 2019, **29**, 1902991.
14 C.-Y. Ke, M.-N. Chen, M.-H. Chen, Y.-T. Li, Y.-C. Chiu and G.-S. Liou, *Adv. Funct. Mater.*, 2021, **31**, 2101288.
15 T. Xu, S. Guo, W. Qi, S. Li, M. Xu and W. Wang, *ACS Appl. Mater. Interfaces*, 2020, **12**, 21952–21960.
16 Q.-B. Zhu, B. Li, D.-D. Yang, C. Liu, S. Feng, M.-L. Chen, Y. Sun, Y.-N. Tian, X. Su, X.-M. Wang, S. Qiu, Q.-W. Li, X.-M. Li, H.-B. Zeng, H.-M. Cheng and D.-M. Sun, *Nat. Commun.*, 2021, **12**, 1798.
17 Z. Shao, T. Jiang, X. Zhang, X. Zhang, X. Wu, F. Xia, S. Xiong, S.-T. Lee and J. Jie, *Nat. Commun.*, 2019, **10**, 1294.
18 Z.-D. Luo, M.-M. Yang, Y. Liu and M. Alexe, *Adv. Mater.*, 2021, **33**, 2005620.
19 M. Carroli, A. G. Dixon, M. Herder, E. Pavlica, S. Hecht, G. Bratina, E. Orgiu and P. Samorì, *Adv. Mater.*, 2021, **33**, 2007965.
20 Y.-C. Lin, W.-C. Yang, Y.-C. Chiang and W.-C. Chen, *Small Sci.*, 2022, 2100109.
21 Y.-H. Chou, H.-C. Chang, C.-L. Liu and W.-C. Chen, *Polym. Chem.*, 2015, **6**, 341–352.
22 Y.-C. Chiang, C.-C. Hung, Y.-C. Lin, Y.-C. Chiu, T. Isono, T. Satoh and W.-C. Chen, *Adv. Mater.*, 2020, **32**, 2002638.
23 H. Chen, Y. Zhou and S.-T. Han, *Nano Sel.*, 2021, **2**, 1245–1265.
24 J.-Y. Chen, Y.-C. Chiu, Y.-T. Li, C.-C. Chueh and W.-C. Chen, *Adv. Mater.*, 2017, **29**, 1702217.
25 J.-S. Lee, *J. Mater. Chem.*, 2011, **21**, 14097–14112.
26 P. Heremans, G. H. Gelinck, R. Müller, K.-J. Baeg, D.-Y. Kim and Y.-Y. Noh, *Chem. Mater.*, 2011, **23**, 341–358.
27 Q. Wang, Y. Xie, F. Soltani-Kordshuli and M. Eslamian, *Renewable Sustainable Energy Rev.*, 2016, **56**, 347–361.
28 Y. Jiang, J. Chen, Y. Sun, Q. Li, Z. Cai, J. Li, Y. Guo, W. Hu and Y. Liu, *Adv. Mater.*, 2019, **31**, 1805761.
29 X. Guo, Y. Xu, S. Ogier, T. N. Ng, M. Caironi, A. Perinot, L. Li, J. Zhao, W. Tang, R. A. Sporea, A. Nejim, J. Carrabina, P. Cain and F. Yan, *IEEE Trans. Electron Devices*, 2017, **64**, 1906–1921.
30 A. Tavasli, B. Gurunlu, D. Gunturkun, R. Isci and S. Faraji, *Electronics*, 2022, **11**, 316.
31 A. K. Tripathi, K. Myny, B. Hou, K. Wezenberg and G. H. Gelinck, *IEEE Trans. Electron Devices*, 2015, **62**, 4063–4068.
32 C.-Y. Ke, M.-N. Chen, Y.-C. Chiu and G.-S. Liou, *Adv. Electron. Mater.*, 2021, **7**, 2001076.
33 Y. Wakayama, R. Hayakawa and H.-S. Seo, *Sci. Technol. Adv. Mater.*, 2014, **15**, 024202.
34 M.-N. Chen, S.-W. Chang, S. P. Prakoso, Y.-T. Li, K.-L. Chen and Y.-C. Chiu, *ACS Appl. Mater. Interfaces*, 2021, **13**, 44656–44662.
35 M.-Y. Liao, Y.-C. Chiang, C.-H. Chen, W.-C. Chen and C.-C. Chueh, *ACS Appl. Mater. Interfaces*, 2020, **12**, 36398–36408.
36 W.-C. Yang, Y.-C. Lin, M.-Y. Liao, L.-C. Hsu, J.-Y. Lam, T.-H. Chuang, G.-S. Li, Y.-F. Yang, C.-C. Chueh and W.-C. Chen, *ACS Appl. Mater. Interfaces*, 2021, **13**, 20417–20426.
37 S. P. Prakoso, S. Kumar, S.-L. Wu, G.-T. Ciou, Y.-J. Ke, S. Venkateswarlu, Y.-T. Tao and C.-L. Wang, *ACS Appl. Mater. Interfaces*, 2020, **12**, 1169–1178.
38 S. P. Prakoso, Y.-J. Ke, D.-C. Huang, C.-L. Wang and Y.-T. Tao, *J. Chin. Chem. Soc.*, 2022, **69**, 440–449.
39 X. Gao, C.-H. Liu, X.-J. She, Q.-L. Li, J. Liu and S.-D. Wang, *Org. Electron.*, 2014, **15**, 2486–2491.
40 E. Ercan, Y.-C. Lin, L.-C. Hsu, C.-K. Chen and W.-C. Chen, *Adv. Mater. Technol.*, 2021, **6**, 2100080.
41 H. Yang, Y. Yan, X. Wu, Y. Liu, Q. Chen, G. Zhang, S. Chen, H. Chen and T. Guo, *J. Mater. Chem. C*, 2020, **8**, 2861–2869.
42 W. Lin, G. Chen, E. Li, L. He, W. Yu, G. Peng, H. Chen and T. Guo, *ACS Appl. Mater. Interfaces*, 2020, **12**, 43967–43975.
43 Y.-F. Yang, Y.-C. Chiang, Y.-C. Lin, G.-S. Li, C.-C. Hung and W.-C. Chen, *Adv. Funct. Mater.*, 2021, **31**, 2102174.
44 H. Chen and J. Fraser Stoddart, *Nat. Rev. Mater.*, 2021, **6**, 804–828.
45 Y. Wang, D. Iglesias, S. M. Gali, D. Beljonne and P. Samorì, *ACS Nano*, 2021, **15**, 13732–13741.
46 Y.-C. Lin, G.-S. Li, P.-J. Yu, E. Ercan and W.-C. Chen, *J. Chin. Chem. Soc.*, 2022, DOI: **10.1002/jccs.202200061**.

47 Y. Yang, Z. Li, C. Wu, W. Li, J. Wang, M. Yi and W. Huang, *J. Mater. Chem. C*, 2022, **10**, 3292–3299.
48 N. Shi, J. Zhang, Z. Ding, H. Jiang, Y. Yan, D. Gu, W. Li, M. Yi, F. Huang, S. Chen, L. Xie, Y. Ren, Y. Li and W. Huang, *Adv. Funct. Mater.*, 2022, **32**, 2110784.
49 S.-H. Yuan, D.-C. Huang and Y.-T. Tao, *ACS Appl. Mater. Interfaces*, 2022, **14**, 7102–7108.
50 C. Xu, J. Zhang, W. Xu and H. Tian, *Mater. Chem. Front.*, 2021, **5**, 1060–1075.
51 A.-C. Chang, Y.-C. Lin, H.-C. Yen, W.-C. Yang, Y.-F. Yang and W.-C. Chen, *ACS Appl. Electron. Mater.*, 2022, **4**, 1266–1276.
52 C.-K. Chen, Y.-C. Lin, J.-C. Ho, W.-C. Yang and W.-C. Chen, *ACS Sustainable Chem. Eng.*, 2022, **10**, 5268–5277.
53 K. Liang, R. Wang, B. Huo, H. Ren, D. Li, Y. Wang, Y. Tang, Y. Chen, C. Song, F. Li, B. Ji, H. Wang and B. Zhu, *ACS Nano*, 2022, DOI: **10.1021/acsnano.2c00439**.
54 L. Zhou, S.-T. Han, S. Shu, J. Zhuang, Y. Yan, Q.-J. Sun, Y. Zhou and V. A. L. Roy, *ACS Appl. Mater. Interfaces*, 2017, **9**, 34101–34110.
55 Y. Yu, Q. Ma, H. Ling, W. Li, R. Ju, L. Bian, N. Shi, Y. Qian, M. Yi, L. Xie and W. Huang, *Adv. Funct. Mater.*, 2019, **29**, 1904602.
56 Y. Wang, L. Kang, Z. Liu, Z. Wan, J. Yin, X. Gao, Y. Xia and Z. Liu, *ACS Appl. Mater. Interfaces*, 2021, **13**, 13452–13458.
57 Q. Li, T. Li, Y. Zhang, Z. Chen, Y. Li, L. Jin, H. Zhao, J. Li and J. Yao, *J. Phys. Chem. C*, 2020, **124**, 23343–23351.
58 M. Yi, J. Shu, Y. Wang, H. Ling, C. Song, W. Li, L. Xie and W. Huang, *Org. Electron.*, 2016, **33**, 95–101.
59 Y.-H. Chang, C.-W. Ku, Y.-H. Zhang, H.-C. Wang and J.-Y. Chen, *Adv. Funct. Mater.*, 2020, **30**, 2000764.
60 J.-Y. Chen, D.-L. Yang, F.-C. Jhuang, Y.-H. Fang, J.-S. Benas, F.-C. Liang and C.-C. Kuo, *Adv. Funct. Mater.*, 2021, **31**, 2105911.
61 Y.-H. Chao, J.-C. Chen, D.-L. Yang, Y.-J. Tseng, C.-H. Hsu and J.-Y. Chen, *Adv. Funct. Mater.*, 2022, 2112521.
62 C.-H. Lin, L. Hu, X. Guan, J. Kim, C.-Y. Huang, J.-K. Huang, S. Singh and T. Wu, *Adv. Mater.*, 2022, 2108616.
63 J. Pei, X. Wu, W.-J. Liu, D. W. Zhang and S.-J. Ding, *ACS Nano*, 2022, **16**, 2442–2451.
64 E. Ercan, J.-Y. Chen, C.-C. Shih, C.-C. Chueh and W.-C. Chen, *Nanoscale*, 2018, **10**, 18869–18877.
65 C.-H. Chen, Y. Wang, T. Michinobu, S.-W. Chang, Y.-C. Chiu, C.-Y. Ke and G.-S. Liou, *ACS Appl. Mater. Interfaces*, 2020, **12**, 6144–6150.
66 E. Ercan, Y.-C. Lin, C.-K. Chen, Y.-K. Fang, W.-C. Yang, Y.-F. Yang and W.-C. Chen, *J. Polym. Sci.*, 2022, **60**, 525–537.
67 S. A. Jenekhe, L. Lu and M. M. Alam, *Macromolecules*, 2001, **34**, 7315–7324.
68 E. Busby, J. Xia, Q. Wu, J. Z. Low, R. Song, J. R. Miller, X. Y. Zhu, L. M. Campos and M. Y. Sfeir, *Nat. Mater.*, 2015, **14**, 426–433.
69 S. P. Prakoso, S.-S. Sun, R. Saleh, Y.-T. Tao and C.-L. Wang, *ACS Appl. Mater. Interfaces*, 2021, **13**, 38365–38374.
70 S. De Feyter and F. C. De Schryver, *Chem. Soc. Rev.*, 2003, **32**, 139–150.
71 A. Ajayaghosh, C. Vijayakumar, V. K. Praveen, S. S. Babu and R. Varghese, *J. Am. Chem. Soc.*, 2006, **128**, 7174–7175.
72 S. Guo, Y. Song, Y. He, X.-Y. Hu and L. Wang, *Angew. Chem., Int. Ed.*, 2018, **57**, 3163–3167.
73 A.-N. Au-Duong, C.-C. Kuo and Y.-C. Chiu, *Polym. J.*, 2018, **50**, 649–658.
74 H.-Y. Chi, H.-W. Hsu, S.-H. Tung and C.-L. Liu, *ACS Appl. Mater. Interfaces*, 2015, **7**, 5663–5673.
75 Y. H. Chou, Y. C. Chiu, W. Y. Lee and W. C. Chen, *Chem. Commun.*, 2015, **51**, 2562–2564.
76 W.-Y. Tung, M.-H. Li, H.-C. Wu, H.-Y. Liu, Y.-T. Hsieh and W.-C. Chen, *Chem. – Asian J.*, 2016, **11**, 1631–1640.
77 P. Cudazzo, M. Gatti and A. Rubio, *Phys. Rev. B: Condens. Matter Mater. Phys.*, 2012, **86**, 195307.
78 J. Lee, S. S. Kim, K. Kim, J. H. Kim and S. Im, *Appl. Phys. Lett.*, 2004, **84**, 1701–1703.
79 H. Chen, X. Wen, J. Zhang, T. Wu, Y. Gong, X. Zhang, J. Yuan, C. Yi, J. Lou, P. M. Ajayan, W. Zhuang, G. Zhang and J. Zheng, *Nat. Commun.*, 2016, **7**, 12512.
80 P. Rivera, J. R. Schaibley, A. M. Jones, J. S. Ross, S. Wu, G. Aivazian, P. Klement, K. Seyler, G. Clark, N. J. Ghimire, J. Yan, D. G. Mandrus, W. Yao and X. Xu, *Nat. Commun.*, 2015, **6**, 6242.
81 T. Zhu, L. Yuan, Y. Zhao, M. Zhou, Y. Wan, J. Mei and L. Huang, *Sci. Adv.*, 2018, **4**, eaao3104.
82 H. Ling, J. Lin, M. Yi, B. Liu, W. Li, Z. Lin, L. Xie, Y. Bao, F. Guo and W. Huang, *ACS Appl. Mater. Interfaces*, 2016, **8**, 18969–18977.
83 J. Ying, J. Han, L. Xiang, W. Wang and W. Xie, *Curr. Appl. Phys.*, 2015, **15**, 770–775.
84 Y. J. Jeong, E. J. Yoo, L. H. Kim, S. Park, J. Jang, S. H. Kim, S. W. Lee and C. E. Park, *J. Mater. Chem. C*, 2016, **4**, 5398–5406.
85 K. Pei, X. Ren, Z. Zhou, Z. Zhang, X. Ji and P. K. L. Chan, *Adv. Mater.*, 2018, **30**, 1706647.
86 Q. Li, Y. Zhang, Y. Yu, Z. Chen, L. Jin, Y. Li, T. Li, Y. Yang, H. Zhao, J. Li, H. Dai, J. Yang and J. Yao, *Nanotechnology*, 2019, **30**, 37LT01.
87 Q. Burlingame, C. Coburn, X. Che, A. Panda, Y. Qu and S. R. Forrest, *Nature*, 2018, **554**, 77–80.
88 C.-W. Tseng, D.-C. Huang and Y.-T. Tao, *ACS Appl. Mater. Interfaces*, 2012, **4**, 5483–5491.
89 S. P. Prakoso, W. S. Feng and K. C. Liu, *2015 IEEE 22nd International Symposium on the Physical and Failure Analysis of Integrated Circuits*, 2015, pp. 350–353, DOI: **10.1109/IPFA.2015.7224404**.
90 M. Januar, S. P. Prakoso, S.-Y. Lan, R. K. Mahanty, S.-Y. Kuo and K.-C. Liu, *J. Mater. Chem. C*, 2015, **3**, 4104–4114.
91 L. Shao, Y. Zhao and Y. Liu, *Adv. Funct. Mater.*, 2021, **31**, 2101951.
92 Q. Liu, S. Gao, L. Xu, W. Yue, C. Zhang, H. Kan, Y. Li and G. Shen, *Chem. Soc. Rev.*, 2022, **51**, 3341–3379.
93 P. Wu, T. He, H. Zhu, Y. Wang, Q. Li, Z. Wang, X. Fu, F. Wang, P. Wang, C. Shan, Z. Fan, L. Liao, P. Zhou and W. Hu, *InfoMat*, 2022, **4**, e12275.

94 Q. Zhang, T. Jin, X. Ye, D. Geng, W. Chen and W. Hu, *Adv. Funct. Mater.*, 2021, **31**, 2106151.
95 L. Janasz, M. Borkowski, P. W. M. Blom, T. Marszalek and W. Pisula, *Adv. Funct. Mater.*, 2022, **32**, 2105456.
96 H. Chen, W. Zhang, M. Li, G. He and X. Guo, *Chem. Rev.*, 2020, **120**, 2879–2949.
97 H. Lee, Y. Won and J. H. Oh, *J. Polym. Sci.*, 2022, **60**, 348–376.
98 C. Li, W. Fan, B. Lei, D. Zhang, S. Han, T. Tang, X. Liu, Z. Liu, S. Asano, M. Meyyappan, J. Han and C. Zhou, *Appl. Phys. Lett.*, 2004, **84**, 1949–1951.
99 L. Shang, Z. Ji, H. Wang, Y. Chen, X. Liu, M. Han and M. Liu, *IEEE Electron Device Lett.*, 2011, **32**, 1451–1453.
100 T. Leydecker, M. Herder, E. Pavlica, G. Bratina, S. Hecht, E. Orgiu and P. Samorì, *Nat. Nanotechnol.*, 2016, **11**, 769–775.
101 Y. Zhou, S.-T. Han, P. Sonar and V. A. L. Roy, *Sci. Rep.*, 2013, **3**, 2319.
102 Y.-C. Chiu, C.-L. Liu, W.-Y. Lee, Y. Chen, T. Kakuchi and W.-C. Chen, *NPG Asia Mater.*, 2013, **5**, e35–e35.
103 C. Qian, J. Sun, L.-A. Kong, Y. Fu, Y. Chen, J. Wang, S. Wang, H. Xie, H. Huang, J. Yang and Y. Gao, *ACS Photonics*, 2017, **4**, 2573–2579.
104 X. Wu, S. Lan, D. Hu, Q. Chen, E. Li, Y. Yan, H. Chen and T. Guo, *J. Mater. Chem. C*, 2019, **7**, 9229–9240.
105 M.-Y. Liao, M. H. Elsayed, C.-L. Chang, Y.-C. Chiang, W.-Y. Lee, W.-C. Chen, H.-H. Chou and C.-C. Chueh, *ACS Appl. Electron. Mater.*, 2021, **3**, 1708–1718.
106 X. Wu, S. Feng, J. Shen, W. Huang, C. Li, C. Li, Y. Sui and W. Huang, *Chem. Mater.*, 2020, **32**, 3641–3650.
107 C. Cai and P. Hou, *IEEE Trans. Device Mater. Reliab.*, 2022, 1, DOI: **10.1109/TDMR.2022.3153961**.
108 H. Yang, Q. Yang, L. He, X. Wu, C. Gao, X. Zhang, L. Shan, H. Chen and T. Guo, *Nano Res.*, 2022, **15**, 386–394.
109 Z. D. Zhang, X. Gao, J. Luo, Y. N. Zhong, J. L. Xu and S. D. Wang, *IEEE Electron Device Lett.*, 2022, **43**, 124–127.
110 X. Zhao, S.-Y. Wei, X.-H. Wang and L.-Z. Qiu, *Adv. Opt. Mater.*, 2021, **9**, 2002256.
111 H. Zhu, C. Fu and M. Mitsuishi, *Polym. Int.*, 2021, **70**, 404–413.
112 D. Zhao, I. Katsouras, M. Li, K. Asadi, J. Tsurumi, G. Glasser, J. Takeya, P. W. M. Blom and D. M. de Leeuw, *Sci. Rep.*, 2014, **4**, 5075.
113 R. C. G. Naber, K. Asadi, P. W. M. Blom, D. M. de Leeuw and B. de Boer, *Adv. Mater.*, 2010, **22**, 933–945.
114 H. Qiu, M. Herder, S. Hecht and P. Samorì, *Adv. Funct. Mater.*, 2021, **31**, 2102721.
115 C. Jo, J. Kim, J. Y. Kwak, S. M. Kwon, J. B. Park, J. Kim, G.-S. Park, M.-G. Kim, Y.-H. Kim and S. K. Park, *Adv. Mater.*, 2022, **34**, 2108979.
116 H. Wang, Q. Zhao, Z. Ni, Q. Li, H. Liu, Y. Yang, L. Wang, Y. Ran, Y. Guo, W. Hu and Y. Liu, *Adv. Mater.*, 2018, **30**, 1803961.
117 B. Yang, Y. Lu, D. Jiang, Z. Li, Y. Zeng, S. Zhang, Y. Ye, Z. Liu, Q. Ou, Y. Wang, S. Dai, Y. Yi and J. Huang, *Adv. Mater.*, 2020, **32**, 2001227.
118 Q. Liu, L. Yin, C. Zhao, Z. Wu, J. Wang, X. Yu, Z. Wang, W. Wei, Y. Liu, I. Z. Mitrovic, L. Yang, E. G. Lim and C. Z. Zhao, *Nano Energy*, 2022, **97**, 107171.
119 Z. Y. Ren, Y. H. Kong, L. Ai, H. Xiao, W. S. Wang, Z. W. Shi and L. Q. Zhu, *J. Mater. Chem. C*, 2022, **10**, 7241–7250.
120 B. Rajendran and F. Alibart, *IEEE J. Emerg. Sel. Top. Circuits Syst.*, 2016, **6**, 198–211.
121 C. Han, X. Han, J. Han, M. He, S. Peng, C. Zhang, X. Liu, J. Gou and J. Wang, *Adv. Funct. Mater.*, 2022, 2113053.
122 J. Shi, J. Jie, W. Deng, G. Luo, X. Fang, Y. Xiao, Y. Zhang, X. Zhang and X. Zhang, *Adv. Mater.*, 2022, 2200380.
123 M. S. Kim, M. S. Kim, G. J. Lee, S.-H. Sunwoo, S. Chang, Y. M. Song and D.-H. Kim, *Adv. Mater. Technol.*, 2022, **7**, 2100144.
124 S. Dai, Y. Zhao, Y. Wang, J. Zhang, L. Fang, S. Jin, Y. Shao and J. Huang, *Adv. Funct. Mater.*, 2019, **29**, 1903700.
125 J. Zhang, S. Dai, Y. Zhao, J. Zhang and J. Huang, *Adv. Intell. Syst.*, 2020, **2**, 1900136.
126 J. Fuller Elliot, T. Keene Scott, A. Melianas, Z. Wang, S. Agarwal, Y. Li, Y. Tuchman, D. James Conrad, J. Marinella Matthew, J. J. Yang, A. Salleo and A. A. Talin, *Science*, 2019, **364**, 570–574.
127 Y. Lee, H.-L. Park, Y. Kim and T.-W. Lee, *Joule*, 2021, **5**, 794–810.
128 Y. van de Burgt, E. Lubberman, E. J. Fuller, S. T. Keene, G. C. Faria, S. Agarwal, M. J. Marinella, A. Alec Talin and A. Salleo, *Nat. Mater.*, 2017, **16**, 414–418.
129 L. Schneider Michael, A. Donnelly Christine, E. Russek Stephen, B. Baek, R. Pufall Matthew, F. Hopkins Peter, D. Dresselhaus Paul, P. Benz Samuel and H. Rippard William, *Sci. Adv.*, 2018, **4**, e1701329.
130 W.-C. Yang, Y.-C. Lin, S. Inagaki, H. Shimizu, E. Ercan, L.-C. Hsu, C.-C. Chueh, T. Higashihara and W.-C. Chen, *Adv. Sci.*, 2022, **9**, 2105190.
131 L. Jiang, C. Xu, X. Wu, X. Zhao, L. Zhang, G. Zhang, X. Wang and L. Qiu, *ACS Appl. Mater. Interfaces*, 2022, **14**, 11718–11726.
132 E. Ercan, Y.-C. Lin, W.-C. Yang and W.-C. Chen, *Adv. Funct. Mater.*, 2022, **32**, 2107925.
133 S. Dai, X. Wu, D. Liu, Y. Chu, K. Wang, B. Yang and J. Huang, *ACS Appl. Mater. Interfaces*, 2018, **10**, 21472–21480.
134 L. Wang, C. Zheng, J. Fu, J. Hua, J. Chen, J. Gao, H. Ling, L. Xie and W. Huang, *Adv. Electron. Mater.*, 2022, 2200155.

